

Check for updates

Plasma-Treated Hydrogel for Combined RONS and Chemotherapy Delivery: A Proof-of-Concept *In Ovo*

Milica Živanić, Albert Espona-Noguera, Angela Privat Maldonado, Patrik Matušů, Francesco Tampieri, Maria-Pau Ginebra, Abraham Lin, Evelien Smits, Annemie Bogaerts, and Cristina Canal*

Oxidative stress-based therapies exploit common cancer traits—elevated reactive oxygen species and altered redox metabolism,-making tumors more susceptible to oxidative damage from, e.g., cold atmospheric plasma, an ionized gas containing reactive oxygen and nitrogen species (RONS). Plasma-treated hydrogels (PTH) emerge as vehicles for RONS delivery. Here, PTH are explored as single vehicle for the combined local delivery of RONS and Doxorubicin (Dox). Dox does not impair PTH function, and its IC50 is lowered in vitro; biological characterization and monotherapy comparison are conducted in ovo. Analysis of over 200 tumors, derived from liposarcoma SW872 or osteosarcoma 143B cell lines, reveals effects in the latter after a single PTH-Dox administration: synergistic GPX4 reduction, with the fraction of high cytoplasmic GPX4 cells dropping from 47% to 24%, and diminished average tumor weight, with multiple tumors (of smaller initial size) weighting 70% less than control. In contrast, mono-therapies enhanced the protective GPX4/NRF2 mRNA or protein expression. GPX4 is a ferroptosis inhibitor linked to therapy resistance. Observing effects after a single PTH-Dox hydrogel administration is exceptional, as indirect plasma treatment has until now required frequent dosing in complex tumor models. For clinical use, multimodal approaches are key, and PTHs offer a convenient platform.

1. Introduction

Despite great advances in oncology, the field remains in need of alternative and adjuvant treatments that can help work around existing challenges. For example, chemotherapies such as Doxorubicin (Dox) are limited by severe, dose-dependent, side effects[1] and cancer resistance.[2-6] While indispensable, systemic administration of chemotherapies limits their efficacy in local tumor management and recurrence prevention at the resection site. In sarcoma care, for instance, this is of critical importance as recurrent cancers are usually seated deeper and are of higher grade, leading to treatment failure.[7-12] Sarcoma management usually involves a combination of surgery with (neo)adjuvant chemotherapy or radiotherapy (multimodal approach) to restrict tumor mass or eliminate residual cells. However, the reported sarcoma local recurrence rate remains high, between 25% and 85%.[7,8] For the mentioned

M. Živanić, A. Espona-Noguera, P. Matušů, F. Tampieri, M.-P. Ginebra, C. Canal

PlasmaMED Lab

Biomaterials

Biomechanics and Tissue Engineering Group

Department of Materials Science and Engineering and Institute for Research and Innovation in Health (IRIS)

Universitat Politècnica de Catalunya BarcelonaTech (UPC)

Av. Eduard Maristany 10-14, Barcelona 08019, Spain

E-mail: cristina.canal@upc.edu

M. Živanić, A. Espona-Noguera, F. Tampieri, M.-P. Ginebra, C. Canal Barcelona Research Center in Multiscale Science and Engineering (CCEM) UPC

Barcelona, Spain



The ORCID identification number(s) for the author(s) of this article can be found under https://doi.org/10.1002/adfm.202502779

© 2025 The Author(s). Advanced Functional Materials published by Wiley-VCH GmbH. This is an open access article under the terms of the Creative Commons Attribution-NonCommercial-NoDerivs License, which permits use and distribution in any medium, provided the original work is properly cited, the use is non-commercial and no modifications or adaptations are made.

DOI: 10.1002/adfm.202502779

M. Živanić, A. P. Maldonado, A. Lin, A. Bogaerts Plasma Lab for Applications in Sustainability and Medicine-Antwerp (PLASMANT)

Department of Chemistry

University of Antwerp

Universiteitsplein 1, Wilrijk, Antwerp 2610, Belgium

A. Espona-Noguera Biosciences Department Faculty of Sciences Technology and Engineering

University of Vic. Central University of Catalonia (UVic-UCC)

Vic, Catalonia 08500, Spain

A. P. Maldonado, A. Lin, E. Smits

Center for Oncological Research (CORE)

Integrated Personalized & Precision Oncology Network (IPPON)

University of Antwerp

Universiteitsplein 1, Wilrijk, Antwerp 2610, Belgium

M.-P. Ginebra, C. Canal

Centro de Investigación Biomédica en Red de Bioingeniería

Biomateriales y Nanomedicina (CIBER-BBN)

Instituto de Salud Carlos III

Madrid 28029, Spain



www.afm-journal.de

reasons, research on local, adjuvant, and alternative therapeutic strategies that can help decrease systemic side effects while improving therapeutic effects, e.g., through cell sensitization or synergistic effects, remains of oncological interest. Using agents that induce a specific type of cell death is a common strategy. One such example are immunogenic cell death (ICD) inducers, which promote the release of damage-associated molecular patterns (DAMPs or danger signals) from cells to help recruit and activate immune cells.[13-16] Another example are agents that help induce or sensitize cells to ferroptosis. Ferroptosis is a recently described, non-apoptotic, cell death pathway that has been linked with therapy resistance in cancer. The key event in ferroptosis is lipid peroxidation in response to elevated levels of oxidants. To protect from oxidative stress and cell death, malignant cells often upregulate the expression of proteins with antioxidant function, e.g., glutathione peroxidase 4 (GPX4) enzyme, which reduces peroxidation of lipids in the membrane to preserve the integrity of the cell and, thus, is regarded as a ferroptosis inhibitor. Agents such as GPX4 inhibitors that can sensitize cells to facilitate ferroptosis are an emerging strategy to reverse resistance in cancer and assist chemotherapies, including Dox, known to elevate oxidants levels in cells.[17-24]

In the described context, cold atmospheric plasma gains interest as a well-tolerated cancer therapy [25-27] that could be used as an adjuvant to help activate anti-tumor immune responses, e.g., via ICD induction, [28] or sensitize cells to treatment, e.g., by overwhelming antioxidant defences. [29] Briefly, cold atmospheric plasma (hereon just plasma) is a weakly ionized gas at nearroom temperature that represents an exogenous source of reactive oxygen and nitrogen species (RONS). RONS are oxidants also produced in different metabolic processes within the cell and are involved in cellular signaling and oxidative stress.[30,31] In malignant cells, RONS levels are commonly elevated, which makes them more sensitive to plasma treatment, i.e., more likely to reach the cytotoxic RONS threshold and die.[32,33] To generate plasma, an electric discharge is applied to a, usually noble, gas to ionize it. There are already several plasma devices certified for medical applications.[34] However, direct plasma treatment requires unrestricted access of the plasma device to the target (tumor tissue). To allow minimally invasive and repeated treatment of anatomically deeper tumors, plasma-treated solutions have been explored. To obtain them, a liquid is exposed to plasma to enrich it with RONS. This is possible as plasma can interact with surrounding molecules (from air, the biological target, or a liquid solution) to generate a complex mixture of reactive species. Most of the generated species are only short-lived due to their high reactivity, but longer-lived RONS (peroxides, nitrites, and nitrates) persist in the plasma-treated solutions.^[35] It has been described that long-lived RONS (in particular H₂O₂ and NO₂-) from plasma can trigger an autoamplificatory multistep process in cancer cells, propagating cell death. [36,37] As such, plasma-treated solutions have been used as a RONS vehicle for indirect plasma treatment of tumors.[38-40] However, scaling up indirect plasma treatment proved to be challenging, with daily administration needed to achieve tumor size reduction in vivo. [41,42] Importantly, with insufficient doses (shorter plasma treatment time = less RONS), plasma-treated liquids were observed to promote tumor growth unless combined with a drug^[42] according to the hormetic effects attributed to RONS. As the field moves toward more translational research, adjuvant and combinatorial strategies have become of central interest.

Plasma-treated hydrogels (PTHs),[28] conceived in our laboratory, emerge as a novel indirect plasma-treatment modality that, compared to easily diluted plasma-treated liquids, can not only ensure precise delivery of RONS to targets and provide a chemically more reactive and biologically active platform, [43-46] but can also provide a very convenient solution to combine RONS with drug delivery in a single delivery vehicle for local applications, as explored here. Briefly, to obtain a PTH, a plasma-treated, thus, RONS-enriched, polymeric solution is crosslinked, entrapping RONS inside the three-dimensional hydrogel network. Hydrogels are porous viscoelastic materials consisting >90% of water (properties highly similar to tissues) and once administered, PTHs can locally release therapeutic RONS via simple diffusion (due to their small size). The PTH field is still in its infancy and so far, there are only a few studies, exploring different polymers and PTH cytotoxicity.[46-51] In our preceding study, we developed and characterized an injectable and shape-adaptable alginate PTH convenient for minimally-invasive and post-surgical applications to irregular cavities. [50] There, we demonstrated for the first time the ability of a PTH treatment to induce ICD, observing upregulation in DAMPs and an enhanced phagocytic uptake of PTH-treated cancer cells in co-culture with human monocyte-derived dendritic cells. Injectable hydrogels as versatile platforms attract attention in biomedical research, with around 30 approved clinically, including one alginate hydrogel for heart failure indications. In cancer, their use is limited, mostly as spacers to protect healthy tissue or aid surgery.^[52] Here, we explore injectable alginate PTH as a therapeutic vehicle for cancer applications.

The aim of this work is to explore the (1) possibility of using PTH as a dual-delivery vehicle for more efficient local tumor management and (2) challenge the PTH-based therapy by using a more advanced in ovo tumor model and compare it with mono-therapy. The in ovo model emerges as a more ethical and high-throughput alternative to the mouse model to reduce the number of animals in preclinical research. In this model, threedimensional and vascularized tumors are grown on the chorioallantoic membrane (CAM) of a fertilized egg, to study cancer cells in a more native-like environment for more translatable research. Importantly, here, we assess the viability of administering the therapeutic hydrogels only once to tumors, in contrast to commonly employed daily injections of plasma-treated liquids, which is not a clinically realistic scenario. This work has three main objectives: (i) to incorporate Doxorubicin to an alginate PTH and assess whether its therapeutic functionality is or not affected (drug integrity, RONS storage and release), (ii) to develop an in ovo sarcoma tumor model to challenge PTH-Dox for a clinically relevant indication, (iii) to perform immunohistochemical analysis of the treated tumor tissues to compare PTH-Dox co-therapy with the respective mono-therapies across general cancer cell death markers (apoptosis, immunogenic cell death, ferroptosis) as these are unexplored for PTHs. This should help assess the feasibility and efficacy, including the eventual synergy, of the co-delivery approach as well as the promising molecular targets to provide rationale and a direction for future, in-depth work on this emerging therapeutic platform.





www.afm-journal.de

2. Results

2.1. Plasma-Derived RONS in Alginate Solution do not Affect the Integrity of Doxorubicin

An injectable alginate PTH was prepared according to our previously optimized protocol. [50] Briefly, 0.5% (w/v) sodium alginate solution was treated with plasma to enrich it with RONS, and then crosslinked into a hydrogel using a crosslinking/retardant agent mixture (CaSO₄/Na₂HPO₄). To investigate the feasibility of using PTH as a single vehicle for the co-delivery of plasmaderived RONS and Dox, two approaches of the free Dox incorporation were tested: an indirect approach, where Dox was mixed after the alginate solution was treated with plasma (PTH-Dox) and a direct approach, where Dox was mixed with an alginate solution and then this mixture was treated with plasma (PTH&Dox) (Figure 1A,i). With the latter approach, already for short plasma treatment times of 2 and 5 min, only 85% and 70% of loaded Dox could be recovered (Figure 1A,i); likely due to partial oxidation of the molecule upon direct exposure to plasma. The oxidation products were either generated in very small concentrations or undetectable by HPLC since in the respective chromatograms, at $\lambda = 210, 270, \text{ and } 480 \text{ nm}, \text{ no additional peaks were observed}$ in respect to control (NTH-Dox, non-treated hydrogel loaded with Dox) (Figure 1A,ii; Figure S1, Supporting Information). In contrast, when Dox was added after the alginate solution was treated with plasma, over 90% of the loaded Dox could be recovered, even for a very long plasma treatment time of 20 min (Figure 1A,i).

2.2. Plasma Treatment and Doxorubicin Incorporation: Enhancing Crosslinking Kinetics and Reducing Storage Modulus in Alginate Hydrogels

The indirect approach to incorporate Dox to PTH was selected for the study, as it was compatible with very long plasma treatment times of alginate solution (Figure 1A), allowing to maximize the enrichment of therapeutic RONS in PTH without compromising the integrity of the drug. This method facilitates more streamlined scaling with plasma treatment and drug dose, when translating from cell culture to more complex tumor models and eventually clinics. [51] Here, the plasma treatment time was 20 min, limited by the water evaporation, with the solution becoming too viscous or the distance of the solution to the plasma plume becoming too large. Due to evaporation, after 20 min of the plasma treatment, 0.5% (w/v) alginate solution was concentrated to 0.91% (w/v). To account for this, all non-treated hydrogels (NTH and NTH-Dox) used in in ovo experiments were prepared using 0.91% (w/v) alginate solution. This adjustment of concentration allowed to obtain non-treated hydrogels with mechanical properties comparable to the plasma-treated hydrogels (PTH and PTH-Dox) (Figure 1B; Figure S1A, Supporting Information), which would otherwise be notably different (see NTH $_{-}C_{0.5}$, black line in Figure 1B).

Different rheological properties were studied to explore the effect of Dox inclusion and very long plasma treatment time (20 min) on alginate hydrogels: frequency sweep, oscillation strain sweep (Figure S1A, Supporting Information), and crosslinking kinetics (Figure 1B). Crosslinking kinetics (or gelation speed, speed of hydrogel formation) was observed as the change of storage (G') and loss (G") modulus over time, with t = 0 min being the hydrogel injection (immediately after the initiation of the crosslinking reaction via the addition of CaSO₄/Na₂HPO₄ to the alginate solution). Hydrogels are viscoelastic materials and G' reflects their solid-like properties (elasticity), whereas G" reflects their liquid-like properties (viscosity). When G' value is higher than G" this indicates a solid-like behavior of the material and once values stabilize, the crosslinking reaction (hydrogel formation) is considered complete. Hydrogels where alginate was treated with plasma (PTH and PTH-Dox) showed notably faster gelation speed, with G' reaching a plateau after around 5 min since hydrogel injection. These hydrogels also showed higher G' at t = 0 min compared to non-plasma-treated hydrogels (NTH and NTH-Dox) where G' values were similar to G" values during the first min (liquid-like behaviour of the hydrogel, very easy injection). However, after 15 min, the G' values of NTH and NTH-Dox rose to match the G' values of PTH and PTH-Dox, and kept growing for the duration of the measurement (30 min). In practical terms, faster complete gelation of plasmatreated hydrogels implies that the physical properties of the hydrogel (e.g., stiffness) are well-defined and not changeable after the hydrogel injection. Although less pronounced, the inclusion of Dox had the same effect as plasma treatment, slightly enhancing the gelation speed of the hydrogel (NTH-Dox > NTH) and lowering the maximum G' of the hydrogel (NTH-Dox < NTH and PTH-Dox < PTH).

2.3. Sequential Delivery of RONS, then Doxorubicin from PTH-Dox Hydrogel

In the design of a dual delivery vehicle, it is important to assess the mutual interaction of the two components. Here, it was of interest to study, on the one hand, the effect of Dox inclusion on RONS concentration and release, and on the other hand, the Dox release profile from PTH (in the presence of RONS) versus NTH (in the absence of RONS) (Figure 1C). First, the concentration of two main long-lived RONS (H2O2 and NO2-) was quantified in the plasma-treated alginate solution with or without Dox, observing no differences due to Dox presence (Figure 1C,i). These RONS were quantified using established colorimetric and fluorescent probes, and electron paramagnetic resonance (EPR) and optical emission spectra (OES) spectra are provided as Figures S2 and S3 (Supporting Information) for more complete characterization of the plasma treatment of alginate solution. Then, to study the release of RONS and Dox, the alginate solutions were crosslinked into hydrogels (PTH, PTH-Dox, and NTH-Dox). The hydrogels were injected in the bottom of a well plate, and PBS was added on top to initiate the release experiment. H₂O₂, NO₂⁻, and Dox were quantified from the release medium at different time points and normalized to their initial concentrations to obtain the release curves in percentage. In line with our previous results, a burst release of RONS was observed, reaching the stationary stage after 30 min.^[50] This RONS release kinetics was unchanged in the presence of Dox, but $\approx 10\%$ less H_2O_2 , and NO_2 could be detected in the release medium, suggesting a possible interaction of Dox with RONS. However, it cannot be excluded that these differences are due to technical limitations when preparing

16163028, 0, Downloaded from https://advanced.onlinelibrary.wiley.com/doi/10.1002/adfm.202502779, Wiley Online Library on [27/08/2025]. See the Terms and Conditions (https://onlinelibrary.wiley.com/terms-and-conditions) on Wiley Online Library for rules of use; OA articles are governed by the applicable Creative Commons Licensean

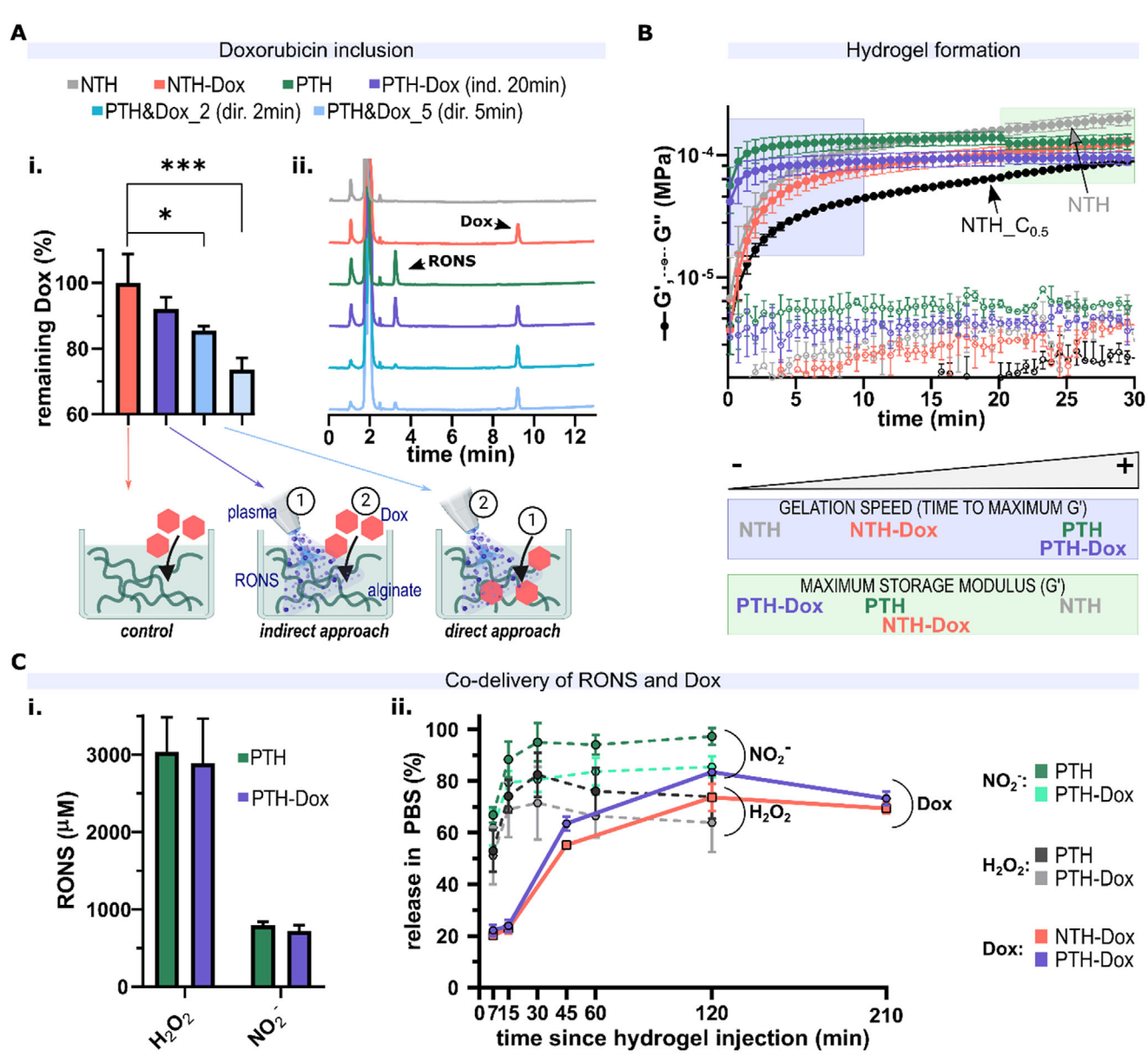


Figure 1. Plasma-treated hydrogel (PTH) as a single vehicle for co-delivery of plasma-derived RONS and Doxorubicin. A) (i) Indirect approach: first, treatment of alginate solution with plasma, then, the addition of Dox (PTH-Dox). Direct approach: first, the addition of Dox to alginate solution, then, treatment of this solution with plasma (PTH&Dox) (n=3). Fraction of loaded Dox that remained after long (20 min) indirect exposure to plasma versus after short (2 or 5 min) direct exposure to plasma. The indirect approach (PTH-Dox) was selected and used in this study. (ii) HPLC-UV chromatograms at 210 nm. Non-treated hydrogel with loaded Dox as control (n=3). B) Effect of long plasma treatment time (20 min) and Dox inclusion on the rheological properties of alginate hydrogels. The change of storage (G') and loss (G'') modulus was followed over time to observe the speed of hydrogel formation and storage modulus after 30 min of the crosslinking initiation. NTH as control. NTH and NTH-Dox were prepared using 0.91% (w/v) alginate to obtain hydrogels comparable to PTH and PTH-Dox (where due to water evaporation during 20 min of plasma treatment, the alginate concentration in solution increases from 0.5% to 0.91%); compared with NTH prepared with 0.5% alginate ($NTH_C_{0.5}$). C) Effect of Dox inclusion on RONS (i) concentration and (ii) release from the PTH (PTH vs PTH-Dox). (ii) Effect of plasma treatment/RONS on Dox release from the hydrogel (NTH-Dox vs PTH-Dox). NTH: non-treated hydrogel. PTH: plasma-treated hydrogel (20 min treatment).

the release calibration curve (see Discussion). Compared to RONS, Dox release from the hydrogel into the release medium was slower, reaching the stationary stage after 2 h, when 80% of the loaded Dox was released. The release kinetics of Dox was not affected by the presence of RONS (*NTH-Dox* versus *PTH-Dox*) (Figure 1C,ii).

2.4. Employing 143B Osteosarcoma and SW872 Liposarcoma Cell Lines for *In Ovo* Tumor Modelling

Two different osteosarcoma cell lines (MG63 and 143B), used in our previous works, $^{[42,46,50]}$ and two soft tissue sarcoma cell lines (SW872 liposarcoma and CCL121 fibrosarcoma) were tested

6163028, 0, Downloaded from https://advanced.onlinelibrary.wiley.com/doi/10.1002/adfm.202502779, Wiley Online Library on [27/08/2025]. See the Terms and Conditions (https://onlinelibrary.wiley.com/terms-and-conditions) on Wiley Online Library for rules of use; OA articles are governed by the applicable Creative Commons Licensean

SCIENCE NEWS

www.afm-journal.de

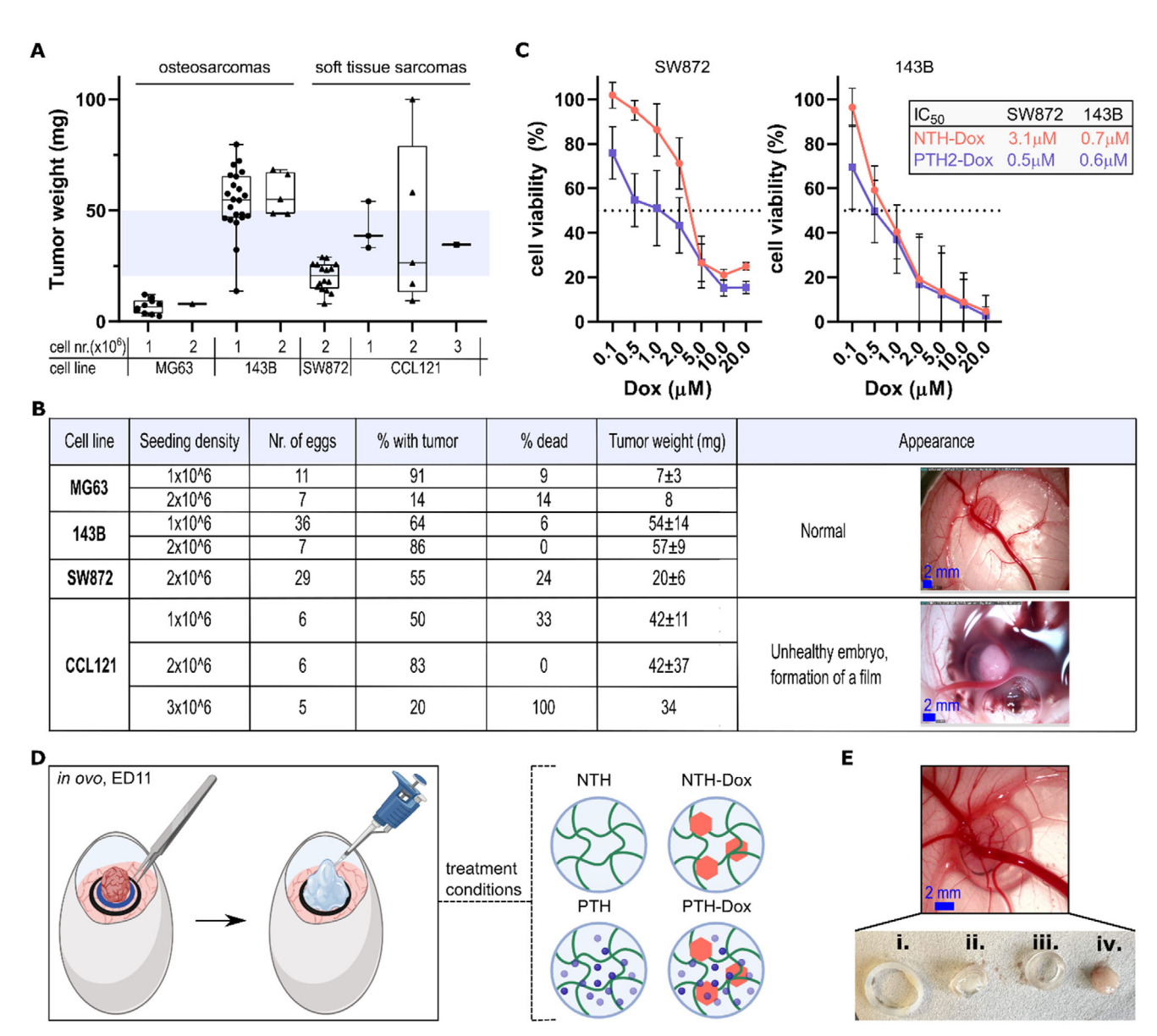


Figure 2. In ovo sarcoma model and experimental design. A) In ovo tumor formation capacity of different sarcoma cell lines at different seeding densities. The blue rectangle indicates the desired range of tumor weight. B) Summary for all in ovo samples used in the course of the study. (A-B) For the two cell lines and seeding densities chosen for this study, the number of eggs is high, as the data from all conducted experiments were pooled together for greater reliability. C) IC50 (half maximum inhibitory concentration) of Doxorubicin in SW872 (liposarcoma) and 143B (osteosarcoma) cells, when Dox was co-delivered with RONS via a 2-min- plasma-treated hydrogel (PTH2-Dox) versus when Dox was delivered via non-treated hydrogel (NTH-Dox). Three biological replicates with three technical replicates each, were performed. D) Experimental design. On embryonic development day 11 (ED11), when tumors were well formed, a plastic ring was placed around the tumor and a therapeutic hydrogel (NTH-Dox, PTH, or PTH-Dox) was administered one time. Controls: NTH, tumors where non-plasma-treated hydrogel was administered, and NT, tumors where no hydrogel was administered. E) On ED13 tumors were weighted and analyzed. Vascularized in ovo tumor (top) and different components retrieved (bottom): (i) outer plastic ring containing (ii) a hydrogel, (iii) inner silicone ring where tumor cells in Matrigel were pipetted to grow (iv) tumor.

for the generation of the in ovo tumor model to be used in the study. Cells were seeded onto the chicken chorioallantoic membrane (CAM) at different densities and two criteria were used to select one cell line from each sarcoma class to be used in this study: (1) high survival rates and healthy appearance of embryo and (2) an average weight of the formed tumor between 20 and 50 mg (Figure 2A,B). The latter is the most commonly found weight range in literature, as it allows for the tumor size that is optimal from the perspective of both downstream manipulation/processing and treatment scale-up. Interestingly, in ovo tumor weight was cell-line specific and did not depend on the seeding density (comparable with).[53] MG63 osteosarcoma cell line generated very small tumors in ovo of average weight below 10 mg for both seeding densities tested (1 and 2 million cells). CCL121 fibrosarcoma cell line was particularly aggressive, leading to the formation of a film-like layer,



www.afm-journal.de

hemorrhage, and high embryo mortality. 143B osteosarcoma and SW872 liposarcoma formed *in ovo* tumors with average weights of 54 and 20 mg, respectively, and were chosen for the study.

2.5. Co-Delivery of Dox and RONS via PTH-Dox Reduces the IC50 Dose of Dox

Prior to the in ovo study, preliminary in vitro experiments were conducted to assess how the cell lines selected for in ovo experiments (SW872 and 143B), respond to Dox as mono- or cotreatment with RONS. For this, Dox was delivered to cells either using non-plasma-treated hydrogel (NTH-Dox) or plasmatreated hydrogel (PTH2-Dox). Different Dox concentrations were loaded in hydrogels, and cell viability was measured 48 h posttreatment to obtain a dose-response curve. For this in vitro experiment, PTH2 (2 min plasma treatment time) was used, since longer plasma-treated hydrogels (with higher concentration of RONS) would kill most/all cells, making it impossible to observe the drug dose-response curve. The IC50 value was determined as the Dox concentration at which half of the maximum cell inhibition was achieved (Figure 2C). The 143B cell line was sensitive to Dox treatment (IC50 = $0.7 \mu M$), with PTH-Dox being slightly more cytotoxic than NTH-Dox for very low Dox concentrations. In contrast, SW872 was more resistant to Dox treatment (IC50 = 3.1 µm) and could be sensitized by co-delivering Dox with RONS via PTH-Dox for a 6-fold reduction in IC50 (IC50 = 0.5 µм; comparable to 143B).

2.6. PTH-Dox Co-Therapy Diminishes Tumor Weight in 143B Osteosarcoma Tumors

The general experimental design of the *in ovo* study is visualized in Figure 2D,E. Briefly, on embryonic development (ED) day 7, sarcoma cells were seeded and, on day 11, the formed tumors were treated by pipetting one of four hydrogel formulations on top so that the tumor was covered: NTH (non-treated hydrogel control), NTH-Dox (Dox mono-therapy), PTH (plasma-derived RONS mono-therapy), or PTH-Dox (co-therapy). All results were compared to non-treated tumors (NT), where no hydrogel was administered. On ED13, tumors were extracted and weighed (Figure 3A,B), and then prepared for downstream analysis. A significant reduction (p < 0.05) in average tumor weight was achieved only for the co-therapy with PTH-Dox in osteosarcoma 143B tumors. Additionally, in the PTH-Dox group, two clusters of tumors could be observed – one comparable to the control and another with 70% lower average weight (Figure 3B, green circle). This could be due to the fact that above a certain weight (probably 50 mg), tumors were too large for the applied therapy dose to be effective (Figure 3B). This highlights the challenge of identifying the correct dose and regimen (necessary RONS and drug concentration, number of administrations) when moving toward more complex preclinical models. Besides tumor size, many other factors can influence the success of the therapy. For example, compared to 143B tumors, SW872 tumors weighed on average 2.5 times less but showed no reduction in weight for any of the applied hydrogel formulations (Figure 3A). These tumors consisted of around 50% of actively proliferating cells, compared to almost 100% for 143B tumors, slightly increased by the therapeutic hydrogels, in line with previous observations^[51] (Figure 3C; Figure S4, Supporting Information). For NTH-Dox and PTH-Dox an increase in cleaved Caspase-3 of 143B cells was observed (p < 0.05) although the total percentage of apoptotic cells remained very low (Figure 3D).

2.7. Expression of Immunogenic Cell Death Markers in Response to PTH Therapy

Immunofluorescence staining of sectioned tumor tissues were performed to detect two cellular markers indicative of ICD: calreticulin (CRT) and heat shock protein 70 (HSP70), both of which promote immune responses against cancer (Figure 4). Images of stained tumor sections were taken via whole-slide fluorescence imaging (Figure 4A, for each condition, multiple SW872 tumors mounted onto a single slide are shown), then processed and analyzed (Figure 4B) to quantify the fraction of cells within the tumor with enhanced expression of ICD markers (Figure 4C,D). Briefly, when analyzing the images, first, the region of interest was annotated - the tumor tissue, excluding chicken cell membrane, necrotic regions, large blood vessels, artifacts, and similar. Then, all cells within the tumor region were detected (based on DAPI nuclear stain) and a fluorescence intensity threshold was applied to classify each cell as positive or negative for the ICD marker (see Figure 4B for example: necrotic cells in the middle of the tumor with unspecific HSP70 staining are excluded from the analysis).

Across all conditions, only a fraction of the treated tumors responded to the therapy with an enhanced expression of ICD markers. High expression of ICD markers was always observed in cells localized on one side of the tumor, likely the one that was in direct contact with the therapeutic hydrogel (see Figure 4B, white arrows). In SW872 tumors, the best results were achieved with PTH mono-therapy, where in half of the observed tumors, \approx 35% of tumor cells showed high CRT expression (compared to \approx 10% and \approx 5% for NT and NTH control groups) (Figure 4C). In some SW872 tumors, HSP70 was also notably upregulated in response to PTH mono-therapy. Interestingly, co-therapy via PTH-Dox performed worse. Similarly, in 143B tumors, PTH mono-therapy, but not PTH-Dox co-therapy, enhanced CRT, so that 10-50% of the cells within the tumor had high CRT expression (compared to \approx 0% for NT and NTH control groups). However, in these tumors, PTH could not promote HSP70 expression. In contrast, HSP70 was upregulated in response to Dox, whereby PTH-Dox performed better than NTH-Dox (Figure 4D).

2.8. PTH-Dox Co-Therapy Synergistically Targets GPX4 Expression in 143B Osteosarcoma Tumors

143B osteosarcoma tumors showed very high expression of GPX4 protein, conferring cells protection against oxidative stress agents such as Dox and RONS (**Figure 5A**, the intensity of brown color is proportional to the concentration of GPX4 protein in the cell). Interestingly, while mono-therapies could not affect GPX4 levels,

16163028, 0, Downloaded from https://advanced.onlinelibrary.wiley.com/doi/10.1002/adfm.202502779, Wiley Online Library on [27/08/2025]. See the Terms and Conditions (https://onlinelibrary.wiley.com/terms-and-conditions) on Wiley Online Library for rules of use; OA articles are governed by the applicable Creative Commons Licenseau Conditions (https://onlinelibrary.wiley.com/terms-and-conditions) on Wiley Online Library for rules of use; OA articles are governed by the applicable Creative Commons Licenseau Conditions (https://onlinelibrary.wiley.com/terms-and-conditions) on Wiley Online Library for rules of use; OA articles are governed by the applicable Creative Commons Licenseau Conditions (https://onlinelibrary.wiley.com/terms-and-conditions) on Wiley Online Library for rules of use; OA articles are governed by the applicable Creative Commons Licenseau Conditions (https://onlinelibrary.wiley.com/terms-and-conditions) on Wiley Online Library for rules of use; OA articles are governed by the applicable Creative Commons Licenseau Conditions (https://onlinelibrary.wiley.com/terms-and-conditions) on Wiley Online Library for rules of use; OA articles are governed by the applicable Creative Commons Licenseau Conditions (https://onlinelibrary.wiley.com/terms-and-conditions) on Wiley Online Library for rules of use; OA articles are governed by the applicable Creative Commons (https://onlinelibrary.wiley.com/terms-and-conditions) on the applicable Creative Commons (https://onlinelibrary.wil

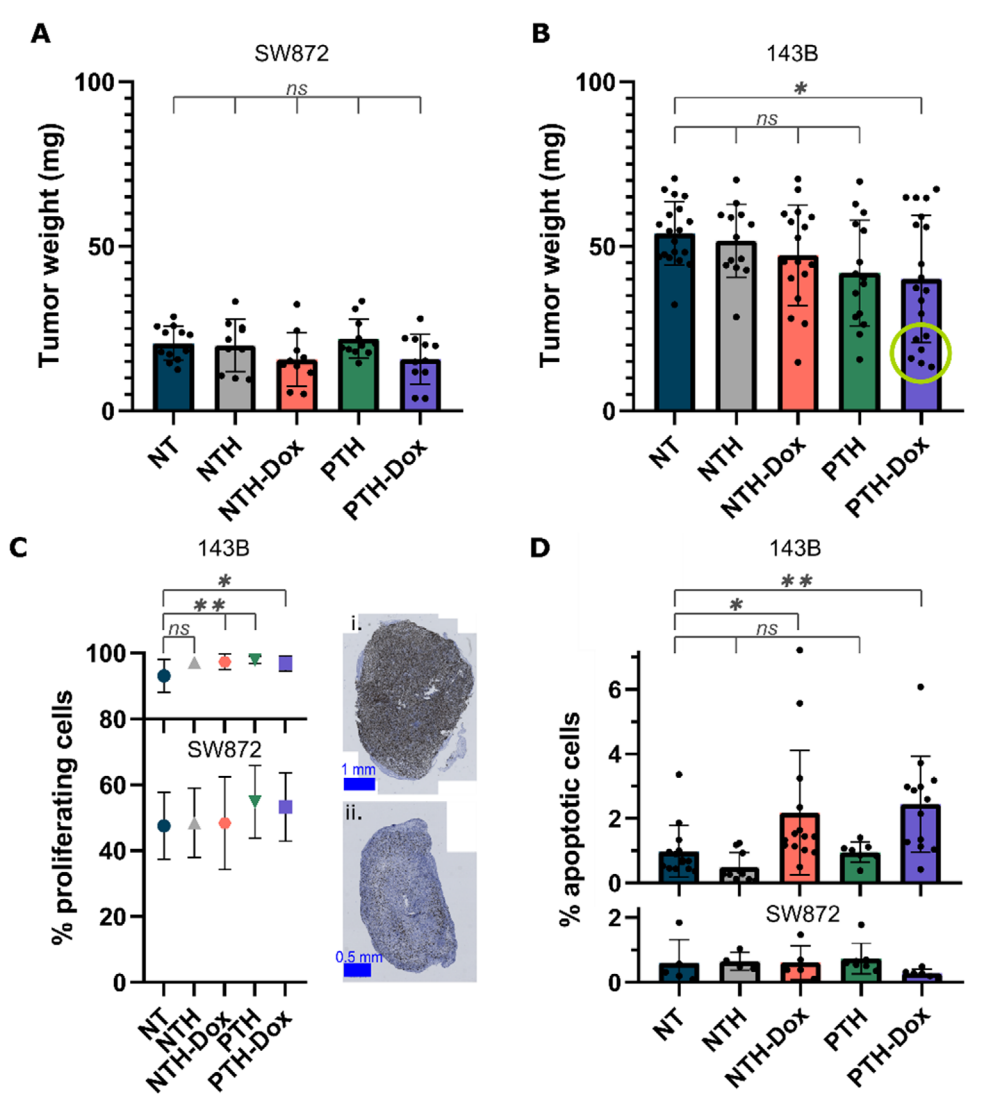


Figure 3. Doxorubicin and RONS mono-/co-treatment of sarcoma tumors via hydrogels. Weight of A) SW872 (liposarcoma) tumors and B) 143B (osteosarcoma) tumors; green circle highlights a group of tumors that responded well to the co-treatment. Statistical test: Welch's ANOVA/Dunnett T3. C) Fraction of cells within the tumor that are actively proliferating and representative images of (i) 143B and (ii) SW872 tumors, immunohistochemistry (brown indicates the presence of Ki67 proliferation marker). Statistical test: Kruskal-Wallis/Dunn. D) Fraction of cells within the tumor that stained positively for cleaved Caspase-3 apoptosis marker. Statistical test: Kruskal-Wallis/Dunn. Control: NT, tumors that were not treated with any hydrogel. NTH: non-plasma-treated hydrogel. PTH: plasma-treated hydrogel. Dox: Doxorubicin. Statistical analysis: comparing all groups against control (NT); ns, non-significant, *p < 0.05, **p < 0.01.

PTH-Dox co-therapy, where Dox was co-delivered with plasmaderived RONS, drastically decreased the expression of GPX4 in tumors, sensitizing them to oxidative stress and ferroptosis. The reduction was quantified via image analysis (Figure 5B). Briefly, after annotating the region of interest in the image, cancer cells were detected and classified based on the intensity of the brown staining (corresponding to GPX4 concentration within the cell): none (blue), low (yellow), medium (orange), and high (red). Additionally, the intensity of the brown staining was observed separately for the cell nucleus and cytoplasm. Thus, one cell could be classified as "red" for nuclear GPX4 (high concentration of the protein in the nucleus) and "yellow" for cytoplasmic GPX4 (low concentration of protein in the cytoplasm) (Figure 5B, an example cell is pointed with a white arrow). GPX4 has different isotypes, each with a cellular compartment preference; for the protection against lipid peroxidation, thus ferroptosis, cytoplasmic GPX4 is of particular interest. The co-therapy via PTH-Dox decreased the fraction of highly GPX4 expressing cells within osteosarcoma 143B tumors – compared to other treatment groups, for PTH-Dox there were $\approx 25\%$ less cells with medium or high *nuclear* GPX4 expression and around 40% less cells with medium or high *cytoplasmic* GPX4 expression (Figure 5C). In fact, for around half of the tumors within the PTH-Dox co-therapy group, $\approx 60\%$ of cancer cells showed no (blue) or only low (yellow) GPX4 expression (Figure 5D, *green circle*). However, despite decreased GPX4, no enhanced lipid peroxidation was observed in these tumors (MDA-staining, Figure S6, Supporting Information), suggesting only sensitization but no activation of ferroptosis was achieved.

16163028, 0, Downloaded from https://advanced.onlinelibrary.wiley.com/doi/10.1002/adfm.202502779, Wiley Online Library on [27/08/2025]. See the Terms and Conditions (https://onlinelibrary.wiley.com/terms-and-conditions) on Wiley Online Library for rules of use; OA articles are governed by the applicable Creative Commons Licensean

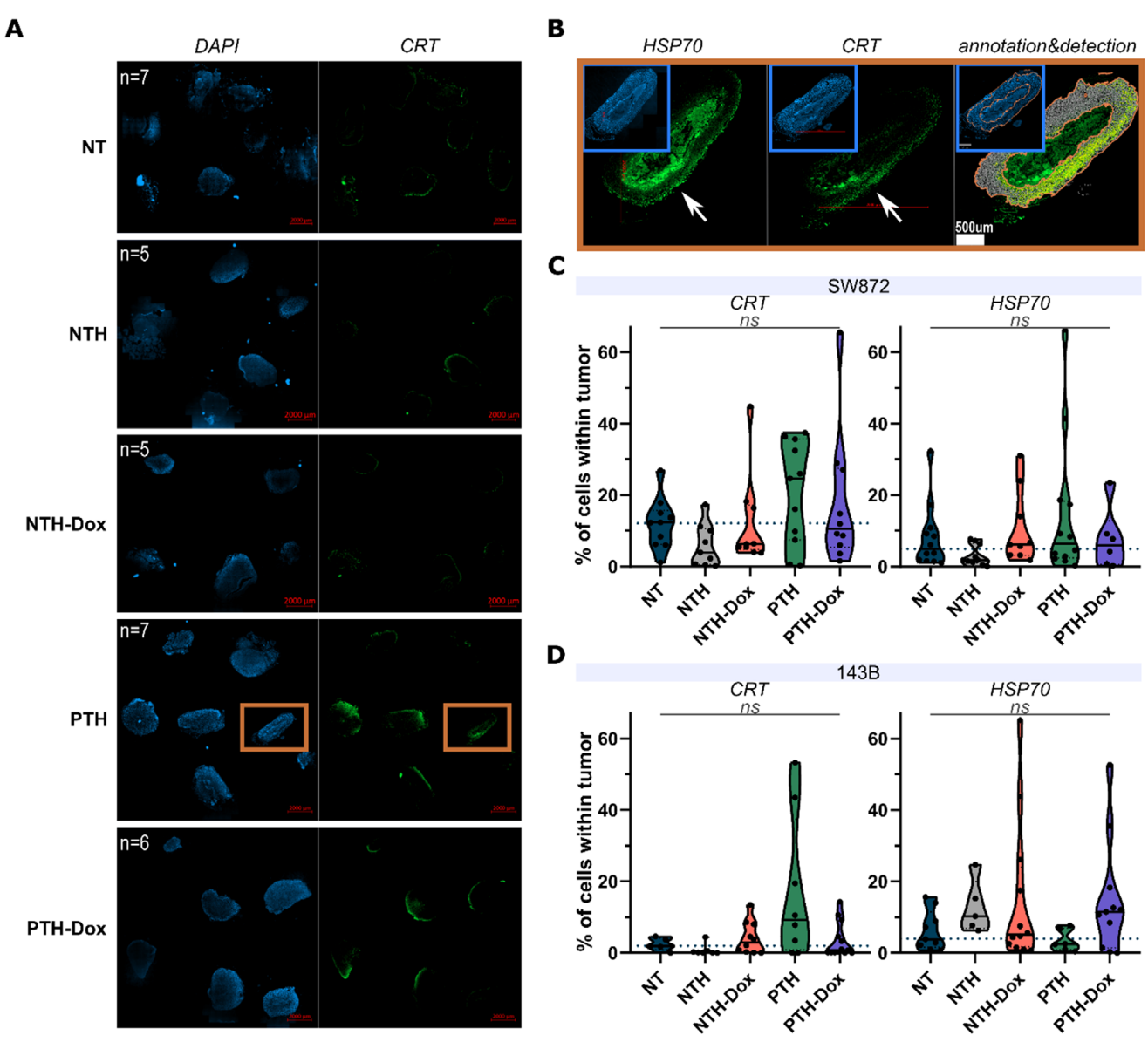


Figure 4. Capacity of Doxorubicin and RONS mono-/co-treatment via hydrogel to induce immunogenic cell death (ICD) in sarcoma tumors. Nuclear staining (DAPI, blue) was used to visualize all cells of the tumor. Calreticulin and Heat Shock Protein 70 (CRT and HSP70, green) were used as molecular markers for ICD. A) Fluorescent images of glass slides carrying multiple SW872 tumors for each treatment condition (n = number of tumors on the slide). Orange rectangle indicates the tumor that is shown in more detail in B). B) To analyze the expression of ICD markers, first, the tumor region of interest was annotated (orange line), excluding chicken membrane, necrotic regions (here the middle) and similar. Then, depending on the intensity of the green channel, each tumor cell was detected as positive (yellow) or negative (grey) for the assigned threshold. For visualization purposes, the background is removed. White arrows indicate that the ICD markers (HSP70 and CRT, separately stained) are present only on one side of the tumor, which was likely in direct contact with the hydrogel. C,D) Summary of results per cell line and ICD marker, expressed as the fraction of tumor cells that are positive for the given marker. Each dot represents a single tumor. Statistical test: Kruskal-Wallis/Dunn. Control: NT, tumors that were not treated with any hydrogel. NTH: non-plasma treated hydrogel. PTH: plasma-treated hydrogel. Dox: Doxorubicin. Statistical analysis: comparing all groups against control (NT), ns: non-significant for p < 0.1.

To exclude compensatory upregulation of the protective NRF2 antioxidant pathway in response to the treatment and decreased GPX4 levels, the mRNA levels of NRF2 and GPX4 were also quantified. NRF2 and GPX4 mRNA levels were indeed upregulated in response to NTH-Dox mono-therapy ($p \le 0.05$). In contrast, their levels were comparable to the control in response to RONS-based PTH mono- and PTH-Dox co-therapy (Figure 5E).

Finally, as for SW872 tumors, neither mono- nor co-therapy influenced GPX4 expression. Moreover, NTH-Dox was comparable to untreated control, whereas in other treatment groups, GPX4 levels were slightly increased. Interestingly, in SW872 cells, GPX4 was mainly localized in the nuclei. Almost 80% of the SW872 cells had no or only low GPX4 expression in the cytoplasm (Figure 5F; Figure S5, Supporting Information).

16163028, 0, Downloaded from https://advanced.onlinelibrary.wiley.com/doi/10.1002/adfm.202502779, Wiley Online Library on [27/08/2025]. See the Terms and Conditions (https://onlinelibrary.wiley.com/terms-and-conditions) on Wiley Online Library for rules of use; OA articles are governed by the applicable Creative Commons Licenseau Conditions (https://onlinelibrary.wiley.com/terms-and-conditions) on Wiley Online Library for rules of use; OA articles are governed by the applicable Creative Commons Licenseau Conditions (https://onlinelibrary.wiley.com/terms-and-conditions) on Wiley Online Library for rules of use; OA articles are governed by the applicable Creative Commons Licenseau Conditions (https://onlinelibrary.wiley.com/terms-and-conditions) on Wiley Online Library for rules of use; OA articles are governed by the applicable Creative Commons Licenseau Conditions (https://onlinelibrary.wiley.com/terms-and-conditions) on Wiley Online Library for rules of use; OA articles are governed by the applicable Creative Commons Licenseau Conditions (https://onlinelibrary.wiley.com/terms-and-conditions) on Wiley Online Library for rules of use; OA articles are governed by the applicable Creative Commons Licenseau Conditions (https://onlinelibrary.wiley.com/terms-and-conditions) on Wiley Online Library for rules of use; OA articles are governed by the applicable Creative Commons (https://onlinelibrary.wiley.com/terms-and-conditions) on the applicable Creative Commons (https://onlinelibrary.wil

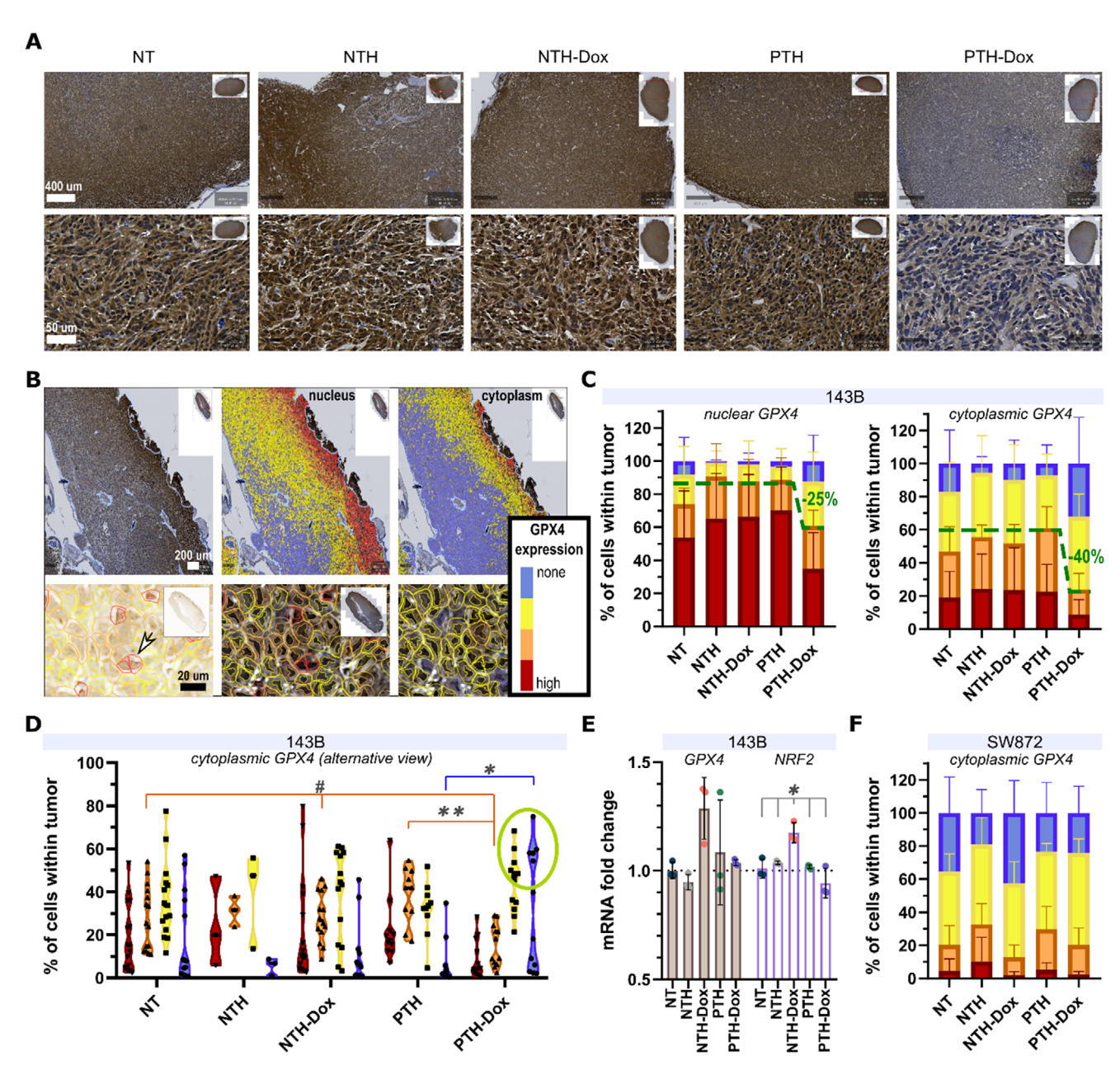


Figure 5. Co-delivery of Doxorubicin and RONS via plasma-treated hydrogel (PTH) could sensitize osteosarcoma tumors to ferroptosis via GPX4 inhibition. A) Representative images of immunohistochemical stainings of tumor sections (brown: GPX4, blue: nuclei). Drastic reduction of glutathione peroxidase 4 (GPX4) expression for PTH-Dox condition. B) Quantification of GPX4 expression per cell compartment (nucleus or cytoplasm). The tumor region of interest is annotated and then, based on the intensity of the brown color, each cell is classified as GPX4 negative (blue), weakly positive (yellow), moderately positive (orange), or very positive with high GPX4 expression (red). If the background is removed, brown color can be seen better (bottom left). The arrow points to an example cell where the nucleus is dark brown and cytoplasm is almost white. Thus, this cell is detected as "red" for nucleus but "yellow" for cytoplasm. C) Summary of the results for 143B (osteosarcoma) tumors. Results are expressed as the fraction of cells within the tumor that are "red", "orange", "yellow", or "blue" (high, moderate, weak, or no GPX4 expression, respectively). D) Alternative representation of results; each dot represents a single tumor. In co-treatment condition (PTH-Dox) there are multiple tumors containing high fraction of cells with weak/no GPX4 expression (green circle). Statistical analysis (Kruskal-Wallis/Dunn or ANOVA/Tukey) was performed for each expression group individually, comparing all conditions: **p < 0.01; *p < 0.05; # p < 0.1. E) mRNA levels of GPX4 and NRF2 in 143B tumors (ANOVA/Tukey; *, p < 0.05). F) Summary of the results for SW872 tumors. Results are expressed as the fraction of cells within the tumor that are "red", "orange", "yellow", or "blue" (high, moderate, weak, or no GPX4 expression, respectively). Control: NT, tumors that were not treated with any hydrogel. NTH: non-plasma treated hydrogel. PTH: plasma-treated hydrogel. Dox: Doxorubicin.



www.afm-journal.de

3. Discussion

In previous works, we developed and optimized injectable alginate-based PTHs as vehicles for the delivery of plasmaderived RONS.[46,50,51] These PTH displayed cytotoxicity toward osteosarcoma cell lines (MG63, 1438, and SaOS2). Furthermore, alginate PTH therapy also enhanced the expression of immunogenic danger signals in cancer cells, which promoted their uptake by immune dendritic cells.^[50] Here, we aimed to challenge the alginate PTH therapy in a more relevant and complex setting, using the in ovo CAM osteosarcoma (a hard tissue sarcoma) and liposarcoma (a soft-tissue sarcoma) tumor model. This model offers a high throughput alternative to in vivo studies, allowing to study vascularized tumors of several millimeters. Previous studies showed that achieving therapeutic doses with plasma-treated liquids in vivo is challenging and usually a daily administration is performed, but this is not a clinically realistic scenario. [42] In inadequate doses, plasma-treated liquids could even promote tumor growth^[42] or treatment resistance through the enrichment of cancer stem cells.^[54] A way to work around these issues is to combine the treatment with another anticancer agent. [42] Generally, the multimodal therapeutic approach is common in oncology, involving a combination of several therapies (e.g., surgery, chemotherapy, radiotherapy...). With potential clinical applications in mind, this work explored the following hypotheses, discussed in more detail in the sections below:

- 1) Drug Incorporation: Can Doxorubicin be incorporated into a PTH system for co-delivery without affecting its function as a RONS vehicle?
- 2) *In Ovo* Translation: Can in vitro results for PTH treatment be replicated in a more challenging and relevant tumor model?
- 3) Synergistic Effects: Does combining and co-delivering Doxorubicin and RONS achieve synergistic therapeutic effects?

3.1. Incorporation of Dox to PTH for Co-Delivery with RONS

When including a drug in a PTH, the capacity of RONS to react with and degrade organic molecules should be considered.[55] Therefore, two possible approaches for the drug inclusion were compared (Figure 1A,i): a) Addition of Dox to the alginate solution after the solution has been exposed to plasma and enriched with RONS (PTH-Dox), or b) Direct generation of RONS in an alginate solution containing Dox (PTH&Dox). Results revealed that the addition of Dox to alginate solution after the treatment, preserved the integrity of the drug even when the solution was exposed to a long plasma treatment (20 min) and, thus, contained high concentrations of plasma-generated RONS. In contrast, when Dox was mixed with alginate before plasma exposure, a significant decrease in detectable Dox was observed within minutes. HPLC-UV/VIS analysis revealed a 15% reduction after 3 min and a 25% reduction after 5 min compared to the non-treated control (NTH-Dox). Taking these results into account, PTH-Dox was selected for subsequent experiments.

Incorporation of Dox did not impair the formation of PTH hydrogel (Figure 1B; Figure S1, Supporting Information) nor its function as RONS vehicle (Figure 1C). Regarding the first, the speed of the hydrogel formation (crosslinking kinetics) was not altered, but the storage modulus of the hydrogel (elastic, solid-

like hydrogel behavior) was slightly lowered due to the presence of Dox. Dox is a bulky planar molecule with multiple rings in its structure and can pose a steric hindrance to the formation of bonds between alginate chains, resulting in a lower crosslinking degree and a more heterogeneous network (lowering the maximum G' of the hydrogel). However, this difference was negligible, not impeding the hydrogel formation. In this study, alginate solution was treated with plasma for a very long time (20 min) to maximize the concentration of therapeutic RONS. In our exploratory in ovo study with pancreatic cancer, PTHs were prepared using 10 min plasma treatment and administered to tumors three times, yet, could not achieve significant therapeutic effects.^[51] Here, the strategy was to maximize the treatment time and introduce Dox, to allow for the rapeutic effects even after a single administration of hydrogel. Such long treatment time did affect the crosslinking kinetics of the hydrogel, leading to complete gelation of plasma-treated hydrogels (PTH and PTH-Dox) in less than 5 min (stabilization of storage modulus), compared to over 30 min for non-plasma treated hydrogels (NTH and NTH-Dox) (Figure 1B). Despite slower kinetics, the storage modulus of non-treated hydrogels (NTH and NTH-Dox) eventually surpassed the one of plasma-treated hydrogels (PTH and PTH-Dox) (Figure 1B). One possible explanation for these observations is the fragmentation of alginate polymer chains to shorter fragments upon their exposure to plasma. Alginate fragmentation and ring opening have been identified as possible outcomes for the interaction between plasma and alginate in solution.^[56] When chains are longer, they provide more bonding sites and span over longer distances within the hydrogel, for a more entangled and stable elastic structure (higher storage modulus).[57] On the other hand, shorter chains have greater freedom and mobility within the solution, and less steric hindrance, which enhances the probability of the contact, alignment, and interaction between the chains for a faster hydrogel formation (time to storage modulus plateau). Another possible mechanism behind the reduction in storage modulus of plasma-treated alginate hydrogels is that the interaction with short-lived RONS could decrease the number of carboxylic groups, responsible for the polymer crosslinking.^[56] Nevertheless, the long plasma treatment times of alginate evaluated here still allowed for the formation of hydrogels with rheological properties comparable to the control, confirming the practicality of employing this polymer for the preparation of PTHs as vehicles for high local delivery of RONS.

Finally, the concentration and release kinetics of RONS were also not affected by the presence of Dox (Figure 1C). The PTH-Dox co-delivery system showed a dual release profile, with a burst release of RONS within 30 min, likely through simple diffusion of these small species, and a slower release of larger Dox molecules, reaching stationary stage after 2 h. Burst of RONS, followed by somewhat delayed drug release, might help sensitize cells to the drug and/or facilitate drug penetration. [58–60] Altogether, we can conclude that the dual Dox and RONS delivery via PTH is a viable option, where none of the functionalities is significantly affected. This study explored the option of directly loading free Dox into the hydrogel in views of simplicity. Different engineering strategies could be explored in the future for a more controlled and sustained drug release. [61]





www.afm-journal.de

3.2. Challenging PTHs in a More Relevant Preclinical Sarcoma Model

Previously, we characterized the alginate PTH used here in the cell culture model, reporting cytotoxicity and immunogenicity for osteosarcoma.^[50] However, in a three-dimensional scaffold environment, osteosarcoma cells have been reported to respond differently and to show greater resistance to the treatment with plasma-treated liquids.[54] Here, we transition to a more advanced and clinically relevant in ovo model, where three-dimensional tumors of several millimeters in diameter are grown on chorioallantoic membrane (CAM), which shares similar properties with the extracellular matrix (ECM) in terms of composition and high vascularization, allowing for a more native-like tumor environment (see Figure 2B,E).[62-64] While this model emerges as a more time and cost-effective alternative to in vivo models and can help refine and reduce the number of animal experiments, it cannot fully replace them, as it is an immunodeficient system with a short experimental window (short follow-up times). In this study, 143B osteosarcoma and SW872 liposarcoma cell lines were used to grow in ovo tumors. As any cell-line derived tumor model, it does not fully replicate the heterogeneity found in patient tumor tissues. Nevertheless, several studies have reported the relevance of cancer cell line-derived in ovo tumors, observing histological properties and treatment responses comparable to in vivo and patient-derived xenografts. [53,63,65] Among the tested cell lines (MG63, 143B, SW872, and CCL121), SW872 and 143B cell lines generated tumors with weight within the desired range of 20-50 mg (Figure 2A,B). The in ovo tumor weight was cellline specific and was not significantly affected by the number of the seeded cells (Figure 2A,B, comparable with ref. [53]). 143B cell line grew in ovo tumors of 54 ± 14 mg, slightly above the desired range and with significant dispersion in the tumor weight (between 45 and 70 mg in the control group). This can affect the efficacy of the treatment, with larger tumors being more resistant than smaller tumors to the applied therapeutic dose. This is likely why, throughout the study, the tumor response can be observed to differ in two groups of tumors (clusters) within the PTH-Dox cotherapy condition - one group of tumors that responded very well to the treatment (70% reduction in tumor weight compared to control average; 60% of GPX4-negative tumor cells) and another one showing only mild/no change in respect to control condition (see Figures 3B and 5D, green circle). Since the starting tumor weight/size (prior to the treatment) is unknown and is only determined is only determined at a single time point, upon the termination of the in ovo study, normalization of the data and more exact interpretation are not possible. However, there appeared to be a certain weight threshold (likely >55 mg), above which the employed therapeutic dose/regimen was insufficient, highlighting the challenge of treatment scale-up when moving toward more complex preclinical tumor models.

When transitioning from two-dimensional cell culture models to three-dimensional models, the penetration of the therapeutic molecule is challenged, the number of cells increases drastically, but also the complexity of cell-cell interactions and communications, which can affect the expression of genes to enhance the resistance to the treatment, as shown also for plasmatreated liquids. [42,54] In addition, the penetration of the therapeutic molecules to the tumor core is challenging. This is why in

all in vivo studies, indirect plasma treatment with plasma-treated liquids is administered repeatedly (usually a daily injection of plasma-treated liquids).[41] However, even this frequency often does not suffice and better results are achieved when combining plasma-treated liquids with drugs.^[42] In contrast to plasmatreated liquids, PTHs are not as easily diluted with body liquids and offer a more localized delivery of RONS for possibly higher therapeutic concentration at the target site. However, our recent study in a well-established pancreatic cancer in ovo model revealed that alginate-based PTHs prepared with 10 min plasmatreated alginate and administered to tumors three times, didn't deliver sufficient concentrations of RONS to achieve a reduction in tumor weight nor affect different tumor properties studied.[51] Thus, here, a longer plasma-treatment time of 20 min was employed to maximize the production of RONS and a Dox drug was introduced into PTH. 20 min was the maximum treatment time reasonable for our setting, limited by the evaporation of the water from the alginate solution (see Section 2.1). The doubling of the treatment time compared to the previous study^[51] increased the H₂O₂ concentration in PTH by 2-fold and the NO₂- concentration by 5-fold. Moreover, the co-delivery strategy allowed to achieve visible and important therapeutic effects (reduction in 143B osteosarcoma tumor weight and GPX4 expression) already after a single administration of the PTH-Dox hydrogel, which is exceptional (see Figures 3B and 5D, green circle). In contrast, mono-therapy with NTH-Dox or PTH could not reduce tumor weight or GPX4 expression. On the other hand, in line with our in vitro results on MG63, 143B, and SaOS2 osteosarcoma cell lines,[50] PTH mono-therapy could enhance the expression of calreticulin (CRT) and heat shock protein 70 (HSP70), which are immunogenic cell death (ICD) and immune-promoting^[66] markers, in 143B osteosarcoma and SW872 liposarcoma in ovo tumors (Figure 4). However, the obtained results on ICD markers are not straightforward to interpret, as: 1) enhanced ICD expression was observed only in a small fraction of tumors; 2) in 143B tumors, HSP70 was not enhanced in response to PTH treatment; 3) the synergy (positive or negative) for PTH-Dox remains unclear as PTH-Dox usually performed worse than PTH (possibly, cell-line and ICD-marker specific); 4) localization of ICD markers (translocation) was not studied; and 5) only semi-quantitative IHC/image analysis was employed. Tumor tissue images interestingly revealed that cancer cells with enhanced ICD expression were always localized on one side of the tumor, likely the one that was in contact with the therapeutic hydrogel (see Figure 4B, white arrow), illustrating the gradient that can be found when treating three-dimensional tumor models. Further studies, including more quantitative methods and immune cells, e.g., immunecompetent mouse models, are needed to validate the immunogenicity of the treatment, i.e., the ability to promote anti-tumor immune responses.

Finally, in vitro, co-delivering Dox with plasma-derived RONS via PTH-Dox allowed to reduce the Dox IC50 dose 6-fold (in the more drug-resistant SW872 cell line), achieving 50% of cell death already at 0.5 μm Dox (compared to 3.1 μm for NTH-Dox) (Figure 2C). This is comparable to a previous work where the combination with plasma-treated medium also reduced the IC50 Dox dose almost 6-fold in prostate cancer cells derived from bone metastasis.^[60] The reduction in IC50 drug dose can be due to plasma treatment-assisted enhanced drug uptake and



www.afm-journal.de

accumulation (e.g., via downregulation of efflux pumps^[60] or upregulation of importer channels)[67] or independent of this, due to additive or synergistic cytotoxic effects. [68,69] The treatment efficacy is challenged when transitioning to 3D models, where cancer cells show altered gene expression and higher resistance.^[54] Despite being able to reduce IC50 drug dose in vitro for SW872 cells (Figure 2C), in ovo, PTH-Dox therapy was not able to reduce liposarcoma tumor weight in these liposarcoma tumors, but only in 143B osteosarcoma tumors, once again, illustrating that it is critical to use advanced tumor models for preclinical characterization and optimization of therapy. Even though 143B tumors were larger and on average 2.5 times heavier than SW872 tumors, PTH-Dox reduced the tumor weight in the first but not in the latter (see Figures 1A and 3C). This is likely related to the fact that the proliferative, thus metabolic activity, of the two observed tumors was very different (50% of cancer cells within SW872 tumors were negative for Ki67 proliferation marker, Figure 3C), but a more in-depth investigation would be needed to test this hypothesis.

3.3. Synergistic Effect of Co-Delivering Dox and Plasma-Derived RONS via PTH-Dox

While mono-therapies (via NTH-Dox and PTH) had no effect, cotherapy via PTH-Dox hydrogel resulted in a significant reduction in tumor weight of 143B osteosarcoma tumors. One-third of the treated 143B tumors weighed ≈70% less than the untreated control (on average 18 mg, compared to 54 mg in the control group) (Figure 3B, green circle). In another third of tumors, some weight reduction was achieved, however, comparable to the PTH group. As discussed in Section 3.2, it appeared that there was a tumor weight threshold (around 50-55 mg), above which the administered therapy was insufficient, challenging the scale-up strategy. However, the fact that the effect on tumor weight could be observed already after a single administration of PTH-Dox to in ovo osteosarcoma tumors is highly significant, given that indirect plasma treatments tested in literature up to now are normally administered multiple times when treating three-dimensional tumors and even this does not guarantee desired results (see Section 3.2).[41,42,51,54] This is why there is a shift toward employing plasma in the context of combinatorial and multimodal approaches, where it is used together with other cancer management strategies, e.g., to help sensitize cells to the treatment or achieve synergistic therapeutic effects.^[29,42]

Related to this, the PTH-Dox co-therapy was able to synergistically target GPX4 protein expression in osteosarcoma tumors (Figure 5). There was a 1.4-fold increase in the fraction of cancer cells with no/low cytoplasmic GPX4 expression in the PTH-Dox co-therapy group. In contrast, monotherapies even had a slightly negative effect (0.7-fold change for PTH and 0.9-fold change for NTH-Dox). As a ferroptosis inhibitor, GPX4 is an emerging target in oncology in the context of sensitizing cells to treatments (reversing drug resistance).^[17–20] It is an important antioxidant protein that together with other proteins confers cells protection against oxidative stress, and, thus, against the therapies that act via this path (such as Dox and plasma), making them ineffective, as it was the case in this study. Cancer cells often upregulate GPX4 and a very high expression was observed in both 143B os-

teosarcoma and SW872 liposarcoma tumors. However, the distribution of GPX4 within the cell compartments was slightly different. In 143B tumors, very high GPX4 expression was detected in the cytoplasm and slightly lower expression in the nucleus (Figure 5C). In SW872 tumors, GPX4 was present only in very small concentrations in the cytoplasm, but in very high in the nucleus of the cells (Figure 5F; Figure S5, Supporting Information). The cytoplasmic GPX4 is of particular importance for ferroptosis where it is responsible for the reduction of lipid peroxidation to protect the integrity of the cell membrane. In response to PTH-Dox co-treatment, the levels of GPX4 protein in osteosarcoma tumors were reduced both in the cytoplasm and the nucleus of 143B osteosarcoma cells (Figure 5C). Furthermore, in PTH-Dox co-therapy group, there were multiple osteosarcoma tumors where ≈60% of the cells were GPX4-negative (Figure 5D, green circle). In contrast, in mono-therapy groups <10% of the cells within the tumor could be classified as negative for cytoplasmic GPX4 expression (Figure 5D). This finding is in agreement with prior reports where direct plasma was combined with temozolomide to inhibit GPX4 expression in glioblastoma spheroids^[70] or with a GPX4-inhibitor (RSL3) to promote ferroptosis in lung cancer cells.^[71] As for the indirect plasma treatment, a plasma-treated cell culture medium was reported to affect several proteins in lung cancer cells that are involved in ferroptosis, but in particular it did not affect the levels of GPX4.[72] In a different approach, plasma-treated liquid was combined with a STAT3-inhibitor (known to also enhance the sensitivity of cells to ferroptosis)[72] to target tumorigenicity.[42] In another study, a plasma-treated liquid and Dox combination was shown to help further decrease antioxidant defenses, including GPX1 that belongs to the same family of proteins as GPX4 but has different functions. [60] Overall, to the best of our knowledge, our study is the first one to report the synergistic effect of combining an indirect plasma treatment (PTH) and chemotherapy to target GPX4 expression.

Decreased GPX4 expression is related to a decreased ability of cells to combat excess peroxidation of lipids in cellular membranes, an event known to trigger ferroptosis.^[73] Ferroptosis is a recently described, non-apoptotic cell death pathway that relies on an iron-dependent Fenton reaction. GPX4 is considered a key repressor of ferroptosis and is the only one in the GPX family of antioxidant proteins that can reduce phospholipid hydroperoxides to the respective alcohols, to prevent their interaction with ferrous iron and, thus, onset of Fenton reaction and generation of further radicals and lipid peroxides.^[74] Induction of ferroptosis, e.g., by inactivation of GPX4, [17] has been shown to sensitize cancer cells to treatment, including osteosarcoma cells.[21,72,75-77] However, we were not able to detect enhanced malondialdehyde, MDA (Figure S6, Supporting Information), which is a marker of lipid peroxidation and ferroptosis, [78] suggesting that, despite sensitization to ferroptosis due to reduced GPX4 expression, no ferroptosis was triggered under the selected treatment regimen.

Finally, interestingly, despite the downregulation of GPX4 protein in response to PTH-Dox therapy, no compensatory increase in cellular mRNA production of GPX4 or NRF2 was observed (Figure 5E). NRF2, short for nuclear factor erythroid 2 (NFE2)-related factor 2, is considered a critical transcriptional regulator of glutathione metabolism (GSH is a cofactor of GPX4) and numerous other factors that protect cells from oxidative stress. Its



www.afm-journal.de

inhibition has been shown to reverse the resistance of cancer to therapies targeting GPX4 and ferroptosis.^[79] The NRF2 pathway is one of the key pathways frequently altered in cancer, contributing to resistance to (chemo)therapies and oxidative stress. [74,80-82] This is well illustrated by our findings, where exposure of osteosarcoma tumors to Dox monotherapy (via NTH-Dox) triggered upregulation of NRF2 and GPX4 mRNA levels in tumors, 48 h after the treatment (Figure 5E). This response likely represents a protective mechanism by the tumor cells to counteract oxidative stress damage and mitigate the effects of chemotherapy. However, thus was not observed for the tumors treated with plasmaderived RONS alone or in combination with Dox (via PTH or PTH-Dox), despite RONS being potent oxidative stress agents. This study is the first to explore, within a broader context, the impact of PTH on antioxidant defenses in cancer. These promising findings open new avenues for research and call for further studies with a more systematic in-depth investigation of this pathway. Collectively, our results suggest that leveraging PTH to co-deliver RONS alongside Doxorubicin could produce certain synergistic effects, effectively re-sensitizing cancer cells to oxidative stress therapies and ferroptosis.

4. Conclusions

This study demonstrates the potential of PTH-Dox as a novel therapeutic strategy for the treatment of sarcoma, where combating local recurrence is critical and current therapeutic strategies are often ineffective and challenged by cancer resistance. The results of the study support the hypothesis that PTH could be used as a single vehicle for localized co-delivery of plasma-derived RONS and a drug (here, Dox) to work around the challenge of indirect plasma treatment scale-up and reduce the systemic drug dose while allowing for improved, synergistic, therapeutic effects. This is supported by the observations that (i) incorporation of Dox into the system did not affect the function of PTH as RONS-vehicle, nor did plasma-derived long-lived RONS compromise Dox integrity, (ii) delivery of Dox via PTH could reduce the cytotoxic IC50 Dox dose by 6-fold in in vitro cell culture, (iii) In contrast to mono-therapies, single administration of co-therapy via PTH-Dox was able to inhibit osteosarcoma tumor growth in ovo (up to 70% lower tumor weight) and to reduce the levels of ferroptosisinhibiting, antioxidative GPX4 protein (up to 40% in the cytoplasm and 25% in the nucleus of cells; in addition, the percentage of GPX4-low/negative cells reached 90% in multiple tumors), while avoiding upregulation of antioxidant defenses at the mRNA level. In addition, this study was able to observe, to some degree, the ability of PTH treatment to enhance the expression of immunogenic cell death signals in in ovo tumors, previously demonstrated in our recent study in cancer cell culture monolayer. Finally, the mentioned therapeutic effects were observed in only a subset of treated tumors, likely of lower initial weight, emphasizing three key challenges in preclinical research: (i) treatment scale-up, (ii) optimization of the dosage and regimen for maximum efficacy, and (iii) identification of the specific clinical indications (tumor types and molecular targets) where the treatment can deliver superior outcomes. Despite these challenges, our findings mark an important step toward refining PTH-based combinatorial therapies, showcasing their potential to overcome resistance mechanisms and improve therapeutic responses in selected tumor types.

5. Experimental Section

Cell Culture: Human osteosarcoma cell lines 143B (ATCC CRL-8303) and MG63 (ATCC CRL-1427), human liposarcoma cell line SW872 (ATCC HTB-92) and human fibrosarcoma cell line CCL121 (ATCC HT-1080) were cultured in DMEM (Thermo Fisher Scientific 10 313 021) supplemented with 10% FBS, 1% Penicillin/Streptomycin, and 2 mm L-Glutamine (complete DMEM).

Plasma Treatment and Preparation Of Hydrogels: Injectable, alginate hydrogels were prepared according to our previously optimized protocol.^[50] Briefly, to prepare plasma-treated hydrogel (PTH), 1 ml of 0.5% w/v sodium alginate solution (PanReac A3245, dissolved in autoclaved deionized water) was added to a 24-well plate and exposed to a plasma source for 20 min (kINPen IND NEOPLAS Tools, operated with high-purity argon gas at 1.1 slm gas flow rate, 10 mm distance, and room temperature, under a sterile hood). After 20 min of plasma treatment, a significant amount of water evaporated so that the final concentration of the alginate solution was 0.91% w/v. Thus, to prepare non-treated hydrogels (NTH), a non-plasma-treated 0.91% w/v alginate solution was used. To crosslink alginate solution into an alginate hydrogel, 20 µL of a crosslinker mixture was added (1:10 v/v). The crosslinker mixture consisted of equal volumes of 1 M CaSO₄·2H₂O crosslinker solution (Merck 1 021 610 500) and 125 mм Na₂HPO₄·2H₂O retardant solution (Fluka BioChemika 71 644), mixed together immediately prior to their addition to the alginate solution. For the preparation of Doxorubicin-containing hydrogels (PTH-Doxo and NTH-Doxo), 20 µL of Doxorubicin HCl solution (Selleckchem #S1208, 240 µm working solution prepared in water on the day of use) was added to 200 µL of plasma-treated or non-plasma-treated alginate solution before adding the crosslinker mixture. Thus, the final concentration of Doxorubicin in the hydrogels was 20 µм. Table 1 summarizes the preparation protocol for different hydrogels used in this study.

Rheology: The crosslinking process (gelation) of all formulations was monitored using a Hybrid Rheometer (Discovery HR-2, TA Instruments) with 20 mm parallel rugous plates configuration. First, a strain sweep (from 0.01 to 10 000% at 1 Hz) and frequency sweep (from 0.1 to 500 Hz at 1% strain sweep) were performed at room temperature to determine the optimal acquisition parameters for the monitoring of gelation time without breaking the hydrogels. To this end, the hydrogel (200 μL) was injected on the rheometer base immediately after the initiation of crosslinking (via addition of the crosslinker mixture), the rheometer arm was lowered to 400 µm gap and after 15 min (when hydrogels are well formed) the measurement was initiated. After the optimization, a frequency of 1 Hz and a strain of 1% were selected for the determination of gelation time. For this, the hydrogel (200 µL) was injected on the rheometer base immediately after the initiation of crosslinking (via addition of the crosslinker mixture), the rheometer arm was lowered to 400 µm gap and immediately the measurement was initiated. In particular, oscillatory measurements were conducted at room temperature and storage (elastic) modulus (G') and the loss (viscous) modulus (G'') were followed for 30 min. The gelation time was defined as the point value where the G' modulus reached the plateau. Three independent replicates were measured.

HPLC: For HPLC analysis, hydrogels (200 μL) containing 20 μm Doxorubicin (Dox) were prepared and left for 24 h in PBS (600 μL) at 37 °C to allow for the maximum release of Dox. Then, the release medium was collected, filtered and analyzed via HPLC. In total 4 different hydrogels were prepared (in triplicates): NTH-Dox (where Dox was mixed with non-treated alginate solution), PTH-Dox (where Dox was mixed with 20-min-plasma treated alginate solution), PTH&Dox_2 (where Dox was mixed with alginate solution and then exposed to plasma for 2 min), and PTH&Dox_5 (where Dox was mixed with alginate solution and then exposed to plasma for 5 min). HPLC/UV-Vis measurements were done using a Shimadzu Prominence XR instrument with autosampler and UV/VIS photodiode array detector equipped with a Agilent 5 TC-C18(2) analytical column (5 μm



www.afm-journal.de

Table 1. Preparation of hydrogels used in this study.

STEP 1. PREPARE ALGINAT	ГЕ	STEP 2. MIX HYDROGEL COMPONENTS			STEP 3. INJECT HYDROGEL
Sodium alginate solution concentration [% w/v]	Plasma treatment [min]	Alginate solution [μL]	Doxorubicin solution [μL]; the final concentration in the hydrogel was 20 μΜ	Crosslinker mixture [µL]; the two components were mixed immediately prior to use	150 μL directly on top of the tumor <i>in ονο</i>
0.91	-	200	-	20	NTH
0.91	-	200	20	22	NTH-Dox
0.5 ^{a)}	20	200	-	20	PTH
0.5 ^{a)}	20	200	20	22	PTH-Dox

a) After 20 min of plasma treatment, due to water evaporation, the concentration of plasma-treated alginate solution becomes 0.91% w/v.

4.6 ×150 mm). Solvent A (0.5 L) was prepared using 1.36 g of Phosphate Buffer (Sigma-Aldrich #71 504) and 0.6 mL of 85% phosphoric acid (Sigma-Aldrich #30 417). Solvent B was acetonitrile. Gradient for B: 1 min isocratic at 25%, increase to 40% in 7 min, 2 min isocratic at 40% and back to 25% in 2 min. The flow rate was 1 mL min-1, temperature 30 °C, detection 190-700 nm and injection volume 20 µL. Under these conditions, the retention time for Dox was 9.20 min. Calibration lines were obtained by analysing, under the same conditions, standard solutions of Dox in PBS. For the calculation of Dox concentration, the area of the peak at 480 nm between 9.0 and 9.5 min was observed. Based on the theoretical Dox concentration in the hydrogel and the assumption that all Dox was released from the hydrogel, the fraction of "preserved" Dox was calculated (Dox that was not affected by the plasma treatment) relative to NTH-Dox control. Since small volumes of solutions were treated (1 mL), water evaporation during the plasma treatment affected the final concentration of Dox in PTH&Dox hydrogels, this was taken into the account.

RONS Quantification: To quantify nitrite ions (NO₂⁻), 50 μL of the sample (here, non-crosslinked plasma-treated alginate solution) was transferred to a transparent 96-well plate and then mixed with 50 µL of the Griess reagent (0.1% w/v of N-(1-naphthyl) ethylenediamine dihydrochloride, 1% w/v of sulphanilamide, and 5% w/v of phosphoric acid in deionized water). Absorbance was measured in a microplate reader at 540 nm and a calibration curve (prepared in the 0.91% w/v alginate solution) was used to calculate the NO₂⁻ concentration. Hydrogen peroxide (H₂O₂) was quantified using Amplex Red/Horseradish peroxidase (AR/HRP)-based fluorescence assay (Sigma). First, the sample was diluted 1:500 in deionized water. Then, 200 μL of the diluted sample was transferred to a black 96-well plate and mixed with 50 μL of AR/HRP solution. The plate was incubated for 30 min at 37 °C. Fluorescence was measured in a microplate reader at $\lambda_{ex}~=~560/20$ nm and $\lambda_{em}~=~590/20$ nm and a calibration curve (prepared in 1:500 diluted 0.91% w/v alginate solution) was used to calculate the H_2O_2 concentration.

RONS and Dox Release: To study the release of NO $_2^-$ and H $_2$ O $_2$ from hydrogel, 200 μ L of hydrogel was pipetted onto a 24-well plate and 1 min later, 1 mL of PBS (Capricorn Scientific, #PBS-1A) was added on top. The plate was incubated at 37 °C. After 7, 15, 30, 60, and 120 min, 50 μ L of the release medium was collected from the well to quantify released NO $_2^-$ by Griess test, and 25 μ L of the release medium was collected and diluted 1:100 to quantify released H $_2$ O $_2$ by AR/HRP assay as described above. At each time point, 75 μ L of fresh PBS was added to the well to compensate for the collected volume.

Similarly, released Dox was detected by sampling 60 μ L of the release medium (600 μ L volume) and measuring the fluorescence ($\lambda_{ex}=485$ nm, $\lambda_{em}=595$ nm). At each time point, 60 μ L of fresh PBS was added to the well to compensate for the collected volume. A calibration curve prepared in PBS was used to calculate the concentration of Dox based on the fluorescence signal. The percentage of released Dox was calculated as the fraction of the theoretical Dox concentration at full release (6.67 μ M).

IC50: Cancer cells were seeded to a 24-well plate 18 h before the treatment: 40 000 cells per well for 143B and 60 000 cells per well for SW872 cell line, in complete DMEM without Sodium-Pyruvate (Thermo Fisher Scien-

tific 31 053 028). To treat cells, the conditioned cell culture medium was removed and 200 µL of Dox-loaded hydrogel was injected directly onto the cells. The hydrogel was either non-treated (NTH-Dox) or 2-minute plasma treated (PTH2-Dox). In line with Table 1, hydrogels were prepared by mixing 200 µL of 0.5% (w/v) non-treated or plasma-treated alginate solution with 20 µL of Dox solution and 22 µL of crosslinker solution. One minute after administering the hydrogel to cells, 1 ml of fresh complete DMEM without Sodium-Pyruvate was added to the well. After 48 h, the hydrogel and conditioned medium were removed and Presto Blue cell viability reagent was added to the cells: 250 μL per well of 1:10 dilution in cell culture medium (Thermo Fisher Scientific P50200). After 1 h of incubation, the Presto Blue reagent was transferred to a black 96-well plate (100 μL/well) and the fluorescent signal was measured ($\lambda_{\rm ex} = 560$ nm, $\lambda_{\rm em} = 590$ nm). IC50 value was calculated as a concentration of Doxorubicin at which the fluorescence (cell viability) decreased by 50% compared to the untreated control

In Ovo: In ovo experiments were performed following a previously described protocol.[51] Briefly, fertilized chicken eggs at the embryonic development day 4 (ED4) were incubated for 1 day in an egg incubator (Ova-Easy 100, Brinsea) at 37.7 °C, 65% humidity, and with automatic rotation mode on. After this, the eggs were stored in an upright position and without rotation. All experimental work on the eggs was performed inside the sterile hood and with the eggs placed on a heat block (37 °C). On ED5, the upper side of the egg was disinfected and punctured using a 20G sterile needle and the hole was sealed with a medical tape. On ED7, cancer cells were pelleted in Eppendorf tubes and stored on ice (1 \times 10⁶ for 143B cells and 2×10^6 for SW872 cells). To seed cancer cells, first the eggshell was cut open. Then, a small cut was made on a well-visible blood vessel by touching the vessel with a filter paper briefly soaked in diethyl ether. Next, a sterile silicone ring (with an inner diameter of 5 mm) was placed on top of the vessel, cancer cells were resuspended in 15 µL of Matrigel $(8.6 \text{ mg mL}^{-1}; \text{Corning})$ and once slightly gelified, pipetted inside the silicone ring. Finally, the egg was sealed using Tegaderm and incubated for 4 more days to allow tumor formation. On ED11, the Tegaderm was cut to access the tumor tissue, another plastic ring was placed around it (inner diameter 7 mm), and hydrogel (150 µL) was pipetted into the ring to treat the tumor. On ED13, tumors were collected, weighted, and processed for downstream analysis. Since in ovo experiments were not conducted beyond ED14, no approval from ethical committee was required. When plotting and discussing tumor weight results, several tumors that weighed over 70 mg were excluded, as well as tumors that were observed to be very small even before the treatment, because here the treatment effect could not be claimed with certainty. For 143B, in total three separate in ovo experiments were conducted and for SW872 two. On average, approximately 40 tumors were extracted after each in ovo experiment.

Histology–Tissue Preparation: Collected tumors were fixed in a 4% paraformaldehyde solution for 24 h and embedded in paraffin following a standard protocol. Paraffin-embedded tumor blocks were sectioned (5 μ m thickness) and these tumor sections were mounted onto glass slides. The slides were baked for 2 h at 60 °C, then stored at 4 °C until staining. Before staining, tissue was deparaffinized and hydrated by immersing the



www.afm-journal.de

Table 2. Conditions and reagents used to perform different histological stainings. IHC: immunohistochemistry. IF: immunofluorescence.

Staining	Antigen	Blocking	Primary antibody	Secondary antibody	Control
IHC	Ki67	2% BSA	Anti-Human Ki-67, MIB-1 (Dako Agilent #M724029-2), 1:75	Universal Dako HRP (EnVision FLEX/HRP Dako Omnis #DM842)	Tonsil tissue
IHC	Cleaved Caspase-3	10% goat serum	Anti-Cleaved Caspase-3, (CellSignTech #9661T), 1:250	Universal Dako HRP (EnVision FLEX/HRP Dako Omnis #DM842)	Tonsil tissue
IHC	GPX4	10% goat serum	Anti-Glutathione Peroxidase, EPNCIR144 (Abcam #ab125066), 1:100	Universal Dako HRP (EnVision FLEX/HRP Dako Omnis #DM842)	Stomach tissue
IF	CRT	10% goat serum	Rabbit IgG monoclonal anti-Calreticulin antibody, EPR3924 (Abcam #ab92516), 1:500	Goat anti-rabbit IgG H&L Alexa Fluor 488 (Abcam #ab150077), 1:1000	Rabbit Ig isotype control (Abcam #ab172730), 1:500
IF	HSP70	10% goat serum	Rabbit IgG monoclonal anti-HSP70 antibody (Abcam #ab181606), 1:50	Goat anti-rabbit IgG H&L Alexa Fluor 488 (Abcam #ab150077), 1:1000	Rabbit Ig isotype control (Abcam #ab172730), 1:50

slides sequentially in xylene (10 min), 100% isopropanol (6 min), 95% isopropanol (6 min), 70% isopropanol (6 min), and MilliQ water (6 min). Then, antigen retrieval was performed using citrate buffer, pH 6.1 (EnVision FLEX target retrieval, Agilent Dako Omnis GV805). Finally, the slides were washed two times to remove the remaining antigen retrieval buffer. All washing steps were performed using a 1X wash buffer (Agilent Dako Omnis GC807) with a detergent (0.025–0.1% Tween or Triton-X). Before starting the staining, the tissue-containing region of the slide was outlined using a PAP pen (Enzo Life Sciences), which helped prevent drying out of tissues during incubation steps.

Tissue Staining: Below, general protocol steps are described and details and antibodies used for each histological staining are indicated in Table 2. To detect Ki67, cleaved Caspase-3, and GPX4, immunohistochemical staining was performed. For this type of staining, the prepared tissues were incubated for 10 min with 3.5% H₂O₂ solution in MilliQ water to block endogenous peroxidases. The slides were then washed and incubated for 40-60 min with a blocking solution. The blocking solution was prepared in the wash buffer and chosen based on the host species of the secondary antibody (see Table 2). After the incubation, the excess blocking buffer was shaken off, and the tissues were incubated for 40-90 min with primary antibody diluted in 1% blocking solution. The slides were then washed and incubated with a secondary antibody for 40 min. In the case of cleaved caspase-3 staining, a linker (EnVision FLEX Rabbit-linker, Dako Omnis GV809) was added for 15 min after the primary antibody and before the secondary antibody to enhance the signal. After the secondary antibody, the slides were washed again, and a freshly prepared DAB chromogen/substrate mixture (EnVision FLEX, Dako Omnis) was added. The signal was developed for 5-10 min. The slides were then washed and the tissues were counterstained with Hematoxylin for 2 min, and rinsed in deionized water. Finally, the slides were dehydrated by immersing them sequentially in 70% isopropanol (2 min), 95% isopropanol (2 min), 100% isopropanol (3 min), and xylene (3 min) and mounted onto glass coverslips for imaging. For each staining, positive and negative (without primary antibody) staining controls were included. To detect CRT and HSP70, immunofluorescence staining protocol was followed. The prepared tissues were incubated for 2 h with a blocking solution. The blocking solution was prepared in the wash buffer and chosen based on the host species of the secondary antibody (see Table 2). After the blocking step, tissues were incubated overnight at 4 °C with primary antibody in 1% blocking solution. Corresponding isotype controls were used. After overnight incubation, the slides were washed well and a secondary antibody diluted in 1% BSA was added to the slides and the slides were incubated at room temperature, protected from the light, for 1 h. Finally, the slides were washed again and mounted onto coverglass using Vectashield HardSet Antifade Mounting medium with DAPI (H-1500) for imaging.

Image Acquisition and Analysis: Whole slide images were acquired only for GPX4 (10x), CRT (SW872), and HSP70 (20x) stainings using ZEISS Axio Scan.Z1. For CRT (143B), images were acquired with ZEISS Axio Ob-

server and tiles were used to image the area of the entire tumor (ZEN software). Images of Ki67 and cleaved Caspase-3 stainings were taken with Leica ICC50 E microscope using the Leica Application Suite EZ. Image analysis was performed using QuPath software. First, a tumor region of interest was annotated, so that chicken cell membrane, necrotic regions, large blood vessels, tissue or staining artifacts were excluded. Next, all tumor cells within the annotations were detected. Finally, detected tumor cells were classified as positive or negative for the specific marker based on the stain intensity. For IHC stainings (Ki67, cleaved Caspase-3, and GPX4), the "positive cell detection" function was used with the parameters as shown in Table 3. For IF stainings (CRT, HSP70), the "cell detection" followed by "single measurement classifier" function was used. For "cell detection" function, the following parameters were used: detection image "DAPI", requested pixel size microns "0.5", background radius microns "8.0", background by reconstruction "true", median radius microns "0", sigma microns "1", minimum cell area microns "27" for 143B tumors or "23" for SW872 tumors, maximum cell area microns "300", threshold "50", watershed post process "true", cell expansion microns "5", include nuclei "true", smooth boundaries "true", make measurements "true". For "single measurement classifier" function, the following thresholds were applied to the cytoplasm compartment: 1900 (CRT 143B), 5600 (CRT SW872), 4800 (HSP70 143B), and 4100 (HSP70 SW872). Cells above this threshold were classified as positive. Images where the staining or tissue appeared faulty were excluded from the analysis.

qPCR: Upon their extraction, tumor tissues were snap frozen in liquid nitrogen. Without allowing for tissues to thaw, they were disrupted with a micro-pestle (Fisher Scientific #16 339 635) and then homogenized using QiaShredder column (Qiagen #79656). The RNA was isolated using RNeasy Mini Kit (Qiagen #74 104). Then the cDNA was synthetized with MaximaFirst Strain cDNA synthesis kit (Fisher Scientific #K1671). qPCR was performed with QuantiNova SYBR Green PCR kit (Qiagen) and using following thermal profile: hot start (95 °C for 2 min), 40 amplification cycles (95 °C for 30 sec, then 65 °C for 10 sec), melt curve (95 °C for 30 sec, then 65 °C for 30 sec). For NRF2 amplification following primer pair was used: CACATCCAGTCAGAAACCAGTGG (forward) and GGAATGTCTGCGCCAAAAGCTG (reverse). For GPX4 amplification, primers were designed to detect all GPX4 isoforms: TGCACGAGTTTTC-CGCCAAG (forward) and CCACGTTGGTGACGATGCAC (reverse).

Statistics and Figures: The statistical analysis was conducted using GraphPad Prism or R software. Where assumptions for parametric tests were met (normality and homogeneity of variance), ordinary one-way ANOVA was used. Where standard deviations were significantly different (Brown-Forsythe <0.05) Welch's ANOVA was used. If normality criteria were not met (Shapiro-Wilk <0.05), a non-parametric Kruskal-Wallis test was used. To correct for multiple comparisons, the recommended post-hoc test was applied (Dunnett, Dunn, Tukey). Statistical tests used and significance levels are specified in the figure's legends and figures. Data is presented as mean \pm SD, with dots representing individual tumor



www.afm-journal.de

Table 3. Parameters used to detect positive cells within IHC stained tumor sections.

Positive cell detection function parameters	143B	SW872	
Detection image	Optical density sum		
Requested pixel size microns	0.5		
Background radius microns	8		
Background by reconstruction	True		
Median filter radius microns	0.5		
Sigma microns	1.5	1.5 for Ki67 and GPX4, 1.0 for cleaved Caspase-3	
Minimum cell area microns	27	23	
Maximum cell area microns	300		
Threshold	0.2	0.5 for Ki67 and GPX4, 2 for cleaved Caspase-3	
Maximum background intensity	2	3 for Ki57 and GPX4, 2 for cleaved Caspase-3	
Cell expansion microns	5		
Include nuclei	True		
Smooth boundaries	True		
Make measurements	True		
Threshold compartment	Nucleus: DAB OD for Ki67 and GPX4, Cell: DAB OD for cleaved Caspase-3, Cytoplasm: DAB OD for GPX4		
Single threshold	True for Ki67 and cleaved Caspase-3, false for GPX4		
Thresholds	0.3 for Ki67, 0.23 for cleaved Caspase-3, 0.3/0.6/0.9 for GPX4	0.3 for Ki67, 0.13 for cleaved Caspase-3, 0.3/0.6/0.9 for GPX4	

tissues. For non-biological experiments, at least 3 replicates were performed. Figures were created using BioRender, Prism GraphPad, and Inkscape.

Supporting Information

Supporting Information is available from the Wiley Online Library or from the author.

Acknowledgements

The authors acknowledge Instituto de Salud Carlos III (ISCIII) and Next Generation EU funds through Project IHRC22/00003 SELLO EXCEL. ISCIII-HEALTH and MINECO though Project PID2022-141120OB-100 funded by MCIU/AEI/10.13039/501100011033/FEDER, UE. MZ, AEN, and CC belong to the SGR2022-1368. Support for the research of CC was received through the ICREA Academia Award for excellence in research, funded by the Generalitat de Catalunya. The authors thank Generalitat de Catalunya for the Scholarship of MZ (2022 FI_B 00532) and COST Action CA20114 (Therapeutical Applications of Cold Plasmas) for the stimulating environment provided and for funding MZ's short-term scientific mission. This work was also partially funded by the Research Foundation—Flanders (FWO) and supported by the following Grant: G004524N (AB and APM) and by a donation of Dedert Schilde vzw (ES). The authors acknowledge technical assistance by Christophe Hermans and fruitful discussions with Dr. J. Tornin.

Conflict of Interest

The authors declare no conflict of interest.

Author Contributions

M.Z., A.E.N., and C.C. performed conceptualization; M.Z., A.E.N., and P.M. performed experimental work; M.Z., A.E.N., F.T., and A.P.M. per-

formed methodology; M.Z., P.M., and F.T. performed data curation; A.E.N., A.P.M., A.L., E.S., A.B., M.P.G., and C.C. performed supervision; C.C., E.S., and A.B. performed funding; M.Z. performed created Figures; M.Z. wrote original draft; all co-authors drafted, reviewed, and edited the manuscript.

Data Availability Statement

The data that support the findings of this study are available from the corresponding author upon reasonable request.

Keywords

cold plasma, combinatorial treatment, doxorubicin, drug delivery, ferroptosis, sarcoma

Received: January 28, 2025 Revised: July 10, 2025 Published online:

- C.-Y. Kong, Z. Guo, P. Song, X. Zhang, Y.-P. Yuan, T. Teng, L. Yan, Q.-Z. Tang, *Int. J. Biol. Sci.* 2022, 18, 760.
- [2] Y. E. Cho, S. C. Kim, H. J. Kim, I. Han, J. L. Ku, J. Transl. Med. 2024, 22, 889.
- [3] B. Das, N. Jain, B. Mallick, Commun. Biol. 2021, 4, 1312.
- [4] B. Gallego, D. Murillo, V. Rey, C. Huergo, Ó. Estupiñán, A. Rodríguez, J. Tornín, R. Rodríguez, *Int. J. Mol. Sci.* 2022, 23, 6425.
- [5] Z. Lin, Z. Fan, X. Zhang, J. Wan, T. Liu, Life Sci. 2020, 263, 118589.
- [6] A. Al Shihabi, P. J. Tebon, H. T. L. Nguyen, J. Chantharasamee, S. Sartini, A. Davarifar, A. Y. Jensen, M. Diaz-Infante, H. Cox, A. E. Gonzalez, S. Norris, J. Sperry, J. Nakashima, N. Tavanaie, H. Winata, S. T. Fitz-Gibbon, T. N. Yamaguchi, J. H. Jeong, S. Dry, A. S. Singh, B.



www.afm-journal.de

- Chmielowski, J. G. Crompton, A. K. Kalbasi, F. C. Eilber, F. Hornicek, N. M. Bernthal, S. D. Nelson, P. C. Boutros, N. C. Federman, J. Yanagawa, et al., *Cell Stem Cell* **2024**, *31*, 1524.
- [7] D. A. Mahvi, R. Liu, M. W. Grinstaff, Y. L. Colson, C. P. Raut, CA Cancer J. Clin. 2018, 68, 488.
- [8] H. Sugiura, S. Tsukushi, M. Yoshida, Y. Nishida, Clin. Orthop. Relat. Res. 2018, 476, 1791.
- [9] J. S. Lin, L. Coleman, R. T. Voskuil, A. Malik, J. L. Mayerson, T. J. Scharschmidt, Arch. Orthop. Trauma Surg. 2024, 144, 2967.
- [10] C. Rodriguez-Galindo, N. Shah, M. B. McCarville, C. A. Billups, M. N. Neel, B. N. Rao, N. C. Daw, Cancer 2004, 100, 1928.
- [11] F. He, W. Zhang, Y. Shen, P. Yu, Q. Bao, J. Wen, C. Hu, S. Qiu, Int. J. Surg. 2016, 36, 283.
- [12] S. Abatzoglou, R. E. Turcotte, A. Adoubali, M. H. Isler, D. Roberge, Clin. Orthop. Relat. Res. 2010, 468, 3012.
- [13] K. I. Arimoto, S. Miyauchi, M. Liu, D. E. Zhang, Front. Immunol. 2024, 15. 1390263.
- [14] F. Shi, X. Huang, Z. Hong, N. Lu, X. Huang, L. Liu, T. Liang, X. Bai, Cancer Lett. 2023. 562. 216167.
- [15] L. Galluzzi, E. Guilbaud, D. Schmidt, G. Kroemer, F. M. Marincola, Nat. Rev. Drug Discovery 2024, 23, 445.
- [16] L. Galluzzi, O. Kepp, E. Hett, G. Kroemer, F. M. Marincola, J. Transl. Med. 2023, 21, 162.
- [17] J. Lee, J. L. Roh, Cancer Lett. 2023, 559, 216119.
- [18] M. J. Hangauer, V. S. Viswanathan, M. J. Ryan, D. Bole, J. K. Eaton, A. Matov, J. Galeas, H. D. Dhruv, M. E. Berens, S. L. Schreiber, F. McCormick, M. T. McManus, *Nature* 2017, 551, 247.
- [19] C. Zhang, C. Wang, Z. Yang, Y. Bai, T. Shukuya, M.-E. Poh, S. Ekman, J. Li, Y. Xu, S. Deng, *Transl. Lung Cancer Res.* 2022, 11, 786.
- [20] Y. Zou, M. J. Palte, A. A. Deik, H. Li, J. K. Eaton, W. Wang, Y.-Y. Tseng, R. Deasy, M. Kost-Alimova, V. Danck, E. S. Leshchiner, V. S. Viswanathan, S. Signoretti, T. K. Choueiri, J. S. Boehm, B. K. Wagner, J. G. Doench, C. B. Clish, P. A. Clemons, S. L. Schreiber, *Nat. Commun.* 2019, 10, 1617.
- [21] C. Zhang, X. Liu, S. Jin, Y. Chen, R. Guo, Mol. Cancer 2022, 21, 47.
- [22] Y. Zhao, Y. Li, R. Zhang, F. Wang, T. Wang, Y. Jiao, Onco Targets Ther. 2020, 13, 5429.
- [23] X. Lu, Q. Zhang, Y. Xie, Cell. Signalling 2023, 110, 110831.
- [24] Y. Tang, Y. He, L. Wu, Pharmgenomics Pers. Med. 2024, 17, 511.
- [25] B. Perillo, M. Di Donato, A. Pezone, E. Di Zazzo, P. Giovannelli, G. Galasso, G. Castoria, A. Migliaccio, Exp. Mol. Med. 2020, 52, 192.
- [26] D. Trachootham, J. Alexandre, P. Huang, Nat. Rev. Drug Discovery 2009. 8, 579.
- [27] M. L. Semmler, S. Bekeschus, M. Schäfer, T. Bernhardt, T. Fischer, K. Witzke, C. Seebauer, H. Rebl, E. Grambow, B. Vollmar, J. Barbara Nebe, H.-R. Metelmann, T. von Woedtke, S. Emmert, L. Boeckmann, Cancers (Basel) 2020, 12, 269.
- [28] M. Zivanic, A. Espona-Noguera, A. Lin, C. Canal, Adv. Sci. (Weinh) 2023, 10, 2205803.
- [29] D. Murillo, C. Huergo, B. Gallego, R. Rodriguez, J. Tornin, Biomedicines 2023, 11, 208.
- [30] H. J. Forman, F. Ursini, M. Maiorino, J. Mol. Cell. Cardiol. 2014, 73, 2.
- [31] H. Sies, D. P. Jones, Nat. Rev. Mol. Cell Biol. 2020, 21, 363.
- [32] S. Arfin, N. K. Jha, S. K. Jha, K. K. Kesari, J. Ruokolainen, S. Roychoudhury, B. Rathi, D. Kumar, Antioxidants (Basel) 2021, 10, 642.
- [33] F. Xing, Q. Hu, Y. Qin, J. Xu, B. Zhang, X. Yu, W. Wang, Front. Oncol. 2022, 12, 862743.
- [34] A. Kazemi, M. J. Nicol, S. G. Bilén, G. S. Kirimanjeswara, S. D. Knecht, Plasma 2024, 7, 233.
- [35] P. J. Bruggeman, M. J. Kushner, B. R. Locke, J. G. E. Gardeniers, W. G. Graham, D. B. Graves, R. C. H. M. Hofman-Caris, D. Maric, J. P. Reid, E. Ceriani, *Plasma Sources Sci. Technol.* 2016, 25, 053002.
- [36] G. Bauer, Redox Biol. 2019, 26, 101291.
- [37] G. Bauer, Redox Biol. 2019, 26, 101301.

- [38] W. Van Boxem, J. Van der Paal, Y. Gorbanev, S. Vanuytsel, E. Smits, S. Dewilde, A. Bogaerts, Sci. Rep. 2017, 7, 16478.
- [39] M. Mateu-Sanz, J. Tornín, B. Brulin, A. Khlyustova, M. P. Ginebra, P. Layrolle, C. Canal, Cancers (Basel) 2020, 12, 227.
- [40] H. Tanaka, K. Nakamura, M. Mizuno, K. Ishikawa, K. Takeda, H. Kajiyama, F. Utsumi, F. Kikkawa, M. Hori, Sci. Rep. 2016, 6, 36282.
- [41] X. Sole-Marti, A. Espona-Noguera, M. P. Ginebra, Cancers (Basel) 2021. 13, 452.
- [42] J. Tornín, M. Mateu-Sanz, V. Rey, D. Murillo, C. Huergo, B. Gallego, A. Rodríguez, R. Rodríguez, C. Canal, Redox Biol. 2023, 62, 102685.
- [43] H. Tanaka, S. Maeda, K. Nakamura, H. Hashizume, K. Ishikawa, M. Ito, K. Ohno, M. Mizuno, Y. Motooka, Y. Okazaki, S. Toyokuni, H. Kajiyama, F. Kikkawa, M. Hori, *Plasma Processes Polym.* 2021, 18, 2100056.
- [44] F. Tampieri, Y. Gorbanev, E. Sardella, Plasma Processes Polym. 2023, 20, 2300077.
- [45] C. Labay, M. Roldán, F. Tampieri, A. Stancampiano, P. E. Bocanegra, M.-P. Ginebra, C. Canal, ACS Appl. Mater. Interfaces 2020, 12, 47256.
- [46] A. Espona-Noguera, F. Tampieri, C. Canal, Int. J. Biol. Macromol. 2024, 257, 128841.
- [47] C. Labay, I. Hamouda, F. Tampieri, M. P. Ginebra, C. Canal, Sci. Rep. 2019, 9, 16160.
- [48] X. Solé-Martí, T. Vilella, C. Labay, F. Tampieri, M.-P. Ginebra, C. Canal, Biomater. Sci. 2022, 10, 3845.
- [49] H. Zhang, S. Xu, J. Zhang, Z. Wang, D. Liu, L. Guo, C. Cheng, Y. Cheng, D. Xu, M. G. Kong, M. Rong, P. K. Chu, Biomaterials 2021, 276, 121057.
- [50] M. Živanić, A. Espona-Noguera, H. Verswyvel, E. Smits, A. Bogaerts, A. Lin, C. Canal, Adv. Funct. Mater. 2024, 34, 2312005.
- [51] A. Espona-Noguera, M. Zivanic, E. Smits, A. Bogaerts, A. Privat-Maldonado, C. Canal, *Macromol. Biosci.* 2024, 24, 2400213.
- [52] A. Mandal, J. R. Clegg, A. C. Anselmo, S. Mitragotri, Bioeng. Transl. Med. 2020, 5, 10158.
- [53] P. Kunz, A. Schenker, H. Sahr, B. Lehner, J. Fellenberg, PLoS One 2019, 14, 0215312.
- [54] J. Tornin, A. Villasante, X. Sole-Marti, M. P. Ginebra, C. Canal, Free Radical Biol. Med. 2021, 164, 107.
- [55] M. Magureanu, N. B. Mandache, V. I. Parvulescu, Water Res. 2015, 81, 124.
- [56] F. Tampieri, A. Espona-Noguera, C. Labay, M.-P. Ginebra, M. Yusupov, A. Bogaerts, C. Canal, Biomater. Sci. 2023, 11, 4845.
- [57] A. Schaur, S. H. Unterberger, R. Lackner, Constr. Build. Mater. 2021, 287.
- [58] Y. Wang, X. Mang, D. Li, Z. Wang, Y. Chen, Z. Cai, F. Tan, Redox Biol. 2024, 69, 102991.
- [59] D. Yan, W. Xu, X. Yao, L. Lin, J. H. Sherman, M. Keidar, Sci. Rep. 2018, 8, 15418.
- [60] M. Mateu-Sanz, M. P. Ginebra, J. Tornin, C. Canal, Free Radical Biol. Med. 2022, 189, 32.
- [61] S. Kumbham, S. Ajjarapu, B. Ghosh, S. Biswas, J. Drug Delivery Sci. Technol. 2023, 87, 104854.
- [62] L. Miebach, J. Berner, S. Bekeschus, Front. Immunol. 2022, 13, 1006064.
- [63] P. Y. Chu, A. P. Koh, J. Antony, R. Y. Huang, Cells Tissues Organs 2022, 211, 222.
- [64] A. Senrung, T. Tripathi, D. Janjua, S. K. Yadav, A. Chhokar, N. Aggarwal, J. Yadav, A. Chaudhary, U. Joshi, P. Sethi, A. C. Bharti, Int. J. Dev. Biol. 2023, 67, 115.
- [65] K. Harper, T. J. Mottram, A. Whitehouse, Cancers (Basel) 2021, 13, 4180.
- [66] I. Mellman, D. S. Chen, T. Powles, S. J. Turley, Immunity 2023, 56, 2188
- [67] S. K. Sagwal, G. Pasqual-Melo, Y. Bodnar, R. K. Gandhirajan, S. Bekeschus, Cell Death Dis. 2018, 9, 1179.

www.advancedsciencenews.com www.afm-iournal.de

- [68] K. Pefani-Antimisiari, D. K. Athanasopoulos, A. Marazioti, K. Sklias, M. Rodi, A.-L. de Lastic, A. Mouzaki, P. Svarnas, S. G. Antimisiaris, Sci. Rep. 2021, 11, 14788.
- [69] K. R. Liedtke, E. Freund, M. Hermes, S. Oswald, C. D. Heidecke, L. I. Partecke, S. Bekeschus, *Cancers (Basel)* 2020, 12, 123.
- [70] P. Shaw, N. Kumar, A. Privat-Maldonado, E. Smits, A. Bogaerts, Cancers (Basel) 2021, 13.
- [71] S. Peng, G. Chen, K. N. Yu, Y. Feng, L. Zhao, M. Yang, W. Cao, W. A. A. Almahi, M. Sun, Y. Xu, Y. Zhao, C. Cheng, F. Zhu, W. Han, Cell Commun. Signalling 2024, 22, 112.
- [72] Q. Liu, K. Wang, Cell Biol. Int. 2019, 43, 1245.
- [73] X. Chen, R. Kang, D. Tang, Front. Cell Dev. Biol. 2021, 9, 646890.
- [74] Q. Zhou, Y. Meng, D. Li, L. Yao, J. Le, Y. Liu, Y. Sun, F. Zeng, X. Chen, G. Deng, Signal Transduction Target Ther. 2024, 9, 55.
- [75] X. Liu, S. Du, S. Wang, K. Ye, Front. Oncol. 2022, 12, 1031779.

- [76] R.-J. Wen, X. Dong, H.-W. Zhuang, F.-X. Pang, S.-C. Ding, N. Li, Y.-X. Mai, S.-T. Zhou, J.-Y. Wang, J.-F. Zhang, *Phytomedicine* **2023**, *116*, 154881.
- [77] C. Qiu, T. Liu, D. Luo, D. Luan, L. Cheng, S. Wang, Front. Oncol. 2022, 12, 746030.
- [78] S. Sun, J. Shen, J. Jiang, F. Wang, J. Min, Signal Transduction Target Ther. 2023, 8, 372.
- [79] D. Shin, E. H. Kim, J. Lee, J. L. Roh, Free Radical Biol. Med. 2018, 129, 454
- [80] D. Li, X. Hong, F. Zhao, X. Ci, S. Zhang, Cancer Cell Int. 2021, 21, 116.
- [81] Y. Huang, W. Yang, L. Yang, T. Wang, C. Li, J. Yu, P. Zhang, Y. Yin, R. Li, K. Tao, Sci. Rep. 2023, 13, 14359.
- [82] X.-J. Wang, Z. Sun, N. F. Villeneuve, S. Zhang, F. Zhao, Y. Li, W. Chen, X. Yi, W. Zheng, G. T. Wondrak, P. K. Wong, D. D. Zhang, *Carcinogenesis* 2008, 29, 1235.